The impact of multidecadal Atlantic meridional overturning circulation variations on the Southern Ocean

Liping Zhang[1& 2] , Thomas L. Delworth[2], and Fanrong Zeng[2]

[1]Atmospheric and Oceanic Science
Princeton University
New Jersey, U.S.

[2]NOAA/Geophysical Fluid Dynamics Laboratory, Princeton
New Jersey, U.S.

Climate Dynamics

Corresponding author address: Liping Zhang, NOAA/Geophysical Fluid Dynamics Laboratory, 201 Forrestal Rd., Princeton, NJ 08540. E-mail: Liping.Zhang@noaa.gov

Abstract

The impact of multidecadal variations of the Atlantic meridional overturning circulation (AMOC) on the Southern Ocean (SO) is investigated in the current paper using a coupled ocean-atmosphere model. We find that the AMOC can influence the SO via fast atmosphere teleconnections and subsequent ocean adjustments. A stronger than normal AMOC induces an anomalous warm SST over the North Atlantic, which favors an increased equator-to-pole temperature gradient in the Southern Hemisphere (SH) upper troposphere and lower stratosphere due to an amplified tropical upper tropospheric warming as a result of increased latent heat release. This eventually strengthens and pushes the Southern Hemisphere westerly jet poleward. The wind change over the SO then cools the SST by anomalous norward Ekman transports. The wind change also weakens the Antarctic bottom water (AABW) cell through changes in surface heat flux heating forcing. The poleward shifted westerly wind decreases the long term mean easterly winds over the Weddell Sea, thereby reducing the turbulent heat flux loss, decreasing surface density and therefore leading to a weakening of the AABW cell. The weakened AABW cell produces a temperature dipole in the SO, with a warm anomaly in the subsurface and a cold anomaly in the surface that corresponds to an increase of Antarctic sea ice. Opposite conditions occur for a weaker than normal AMOC. Our study here suggests that efforts to attribute the recent observed SO variability to various factors should take into consideration not only local process but also remote AMOC forcing.

1. Introduction

The Atlantic Meridional Overturning Circulation (AMOC) plays a crucial role in the global climate system, characterized by a northward flow of warm and salty water in the upper layer of the Atlantic, and a southward flow of cold water in the deep Atlantic (e.g. Bryden et al. 2005; Wunsch and Heimbach 2006). The AMOC transports a large amount of heat from the Southern Hemisphere (SH) and Tropics to the North Atlantic where the heat is released to the atmosphere (e.g. Delworth et al. 2008). This AMOC-induced anomalous northward heat transport favors generating a north-south sea surface temperature (SST) dipole across the Atlantic equator (e.g. Delworth et al. 1993; Zhang and Delworth 2005; Knight et al. 2005; Wu et al. 2008; Zhang and Wang 2013), which is frequently used to explain the Atlantic multidecadal oscillation (AMO) (e.g. Folland et al. 1984; Gray et al. 1997; Delworth and Mann 2000; Wang and Zhang 2013; Zhang and Wang 2013).

Changes in the AMOC have a profound impact on the Northern Hemispheric and Tropical climate system. Paleoclimate records and North Atlantic waterhosing experiments showed that a weakening of AMOC is associated with colder than nrmal temperature over Europe and the U.S., a southward shift of the Atlantic intertropical convergence zone (ITCZ) as well as decreased Indian/Sahel precipitation and Atlantic hurricane activity (e.g. Black et al. 1999; Peterson et al. 2000; Vellinga et al. 2002; Zhang and Delworth 2005; Stouffer et al. 2006; Wu et al. 2008). The AMOC change induces significant responses outside the Atlantic as well, including the tropical Pacific El Niño-Southern Oscillation (ENSO) (e.g. Dong and Sutton 2002; Timmermann et al. 2005; Dong and Sutton 2007), summer Asian and Indian monsoon

(Wang et al. 2001; Altabet et al. 2002), river runoff to the Cariaco Basin (Wang et al. 2004), and North Pacific temperature (Timmermann et al. 2007; Wu et al. 2008; Zhang and Delworth 2005). In contrast, few studies focused on the impact of AMOC on the SH, particularly on the Southern Ocean (SO).

The impact of AMOC on the SH is commonly related to the bipolar seesaw in temperature anomalies (e.g. Crowley 1992; Stocker et al. 1992; Knight et al. 2005; Stouffer et al. 2007; Delworth and Zeng 2012). It is argued that changes in the strength of the AMOC would lead to warming of one hemisphere while the other cools due to the anomalous northward heat transport. This out of phase relationship between the North Atlantic and the Antarctic temperature is also revealed by many indirect proxy records (e.g. Blunier and Brook 2001; Broecker 1998, 2000; Weaver et al. 2003). Broecker (1998, 2000) hypothesized that these paleoclimate bipolar seesaw phenomena reflect an alternation of deep formation in the two hemispheres, where an enhanced North Atlantic deep water (NADW) formation leads to a weakened Antarctic bottom water (AABW) formation and vice versa. Based on a simple paleoclimate model, Weaver et al. (2003) verified that a weakening of AABW by freshening the southern high latitudes could lead to a switch of the AMOC from an "off" to an "on" state. Stouffer et al. (2007) and Swingedouw et al. (2009) further pointed out that the SO freshwater initially triggers a spin up of the AMOC in a complicated climate model, however, the freshwater can spread to the North Atlantic region several decades later, eventually leading to a spin down of the AMOC. Stouffer et al. (2007) also suggested that the North Atlantic freshwater input that leads to a

84 weakening of the AMOC produces a slight warming in the SH, but has a very small or
85 no impact on the AABW formation. Latif et al. (2013) and Martin et al. (2013)
86 demonstrated that the SO deep water convection and SST have their own centennial
87 internal variability that is independent of other internal variability and forced forcing,
88 which contribute some to the recent decadal trends observed in the SH. This internal
89 variability may be superimposed on the AMOC-triggered AABW variability, which
90 could offset the potential effect of AMOC on the AABW to some extent. Therefore,
91 whether the AMOC influences the AABW or not is still not clear yet, particularly in
92 the current climate.

93 Here we use a fully coupled climate model GFDL CM2.1 (Delworth et al. 2006)
94 with fixed preindustrial forcing to comprehensively study the SO response to the
95 multidecadal AMOC variations. In addition to surface air temperature and SST that
96 was addressed by previous studies (e.g. Zhang and Delworth 2005; Stouffer et al.
97 2006; Stouffer et al. 2007), we specifically pay attention to the SO subsurface
98 temperature, deep water formation, wind driven circulation, and sea ice change
99 induced by the AMOC. We attempt to address by which path the multidecadal AMOC
100 variations can influence the SO and what the potential mechanisms are behind this
101 influence. We also try to address to what extent recently observed SO variability can
102 be attributed to the AMOC influence.

103 The paper is organized as follows. Section 2 briefly describes the coupled model,
104 sensitivity experiments design, observational datasets as well as reanalysis data. The
105 simulated SO response to the multidecadal AMOC fluctuations is presented in section

106 3. Possible mechanisms controlling the SO response to the multidecadal AMOC are
107 examined in section 4. In section 5, we investigate the potential linkages of recent SO
108 cooling with the AMOC. Discussion and summary are given in section 6.

109 **2. Model description, experimental design and datasets**

110 The coupled model used in this study is Geophysical Fluid Dynamics Laboratory
111 (GFDL) CM2.1 (Delworth et al. 2006). The atmospheric model has a horizontal
112 resolution of 2.5^{o} in longitude and 2.0^{o} in latitude, with 24 levels in the vertical. The
113 horizontal resolution of the ocean model is 1^{o} in the extratropics, with finer
114 meridional grid-spacing in the tropics (~1/3^{o}). The ocean model has 50 levels in the
115 vertical, with 22 evenly spaced levels over the top 220 m. The coupled model runs for
116 2000-year with atmospheric constituents and external forcing held constant at 1860.

117 We wish to assess how the SO responds to multidecadal AMOC variations. Here
118 we use an idealized 100-yr periodic North Atlantic Oscillation (NAO, Hurrell 1995)
119 forcing to trigger multidecadal AMOC variations. Previous studies have pointed out
120 that the NAO can lead to significant responses in the AMOC (e.g. Delworth and
121 Dixon 2000; Lohmann et al. 2009), with a positive (negative) NAO phase
122 corresponding to a spin up (spin down) of AMOC. The positive NAO-related fluxes,
123 mainly the heat flux, tend to extract more heat from the North Atlantic Ocean, thereby
124 cooling and increasing the density of the upper ocean and thus leading to a
125 strengthening of the AMOC and vice versus. The anomalous NAO forcing used in this
126 study comes from the ECMWF-Interim reanalysis (Dee et al. 2011), as well as the
127 time series of the observed NAO using a station-based index (downloaded from the

NCAR/UCAR climate data guide at https://climatedataguide.ucar.edu/climate-data/hurrell-north-atlantic-oscillation-nao-index-station-based). We compute 4-month averages over the December-March period. Fig. 1 shows the regression map for surface heat flux anomalies associated with a one standard deviation increase in the NAO. The anomalous heat flux forcing is only over the North Atlantic from the equator to 82^{o}N, including the Barents and Nordic Seas. The area integral of the heat flux is constrained to be zero, so that there is no net addition of heat to the system.

The coupled model normally computes air-sea fluxes of heat, water and momentum that depend on the gradients in these quantities across the air-sea interface. In our perturbation experiment this process continues, but after these fluxes are calculated we add an additional flux component to the model ocean. The model ocean therefore "feels" the fluxes that are computed based on air-sea gradients, plus an extra flux that corresponds to an idealized NAO heat flux which has the spatial pattern in Fig. 1 and has the amplitude modulated sinusoidally in time with a 100-yr period. The NAO forcing is applied only in the months of December through March, with a linear taper at the start and end of this period. It is worth noting that the atmospheric model cannot directly feel these altered heat flux. The atmosphere is only impacted through any changes to the ocean that the NAO-related heat flux anomalies induce.

In brief, we conduct two parallel ten-member ensembles of simulations, with each simulation extending for 300 years. The first ensemble is a set of control simulations, with atmospheric composition and radiative forcing fixed at preindustrial

conditions. The second ensemble is identical, except that for each simulation the additional NAO-related heat flux forcing is applied to the ocean component of the model. The difference between the ensembles is interpreted as the influence of the NAO-related fluxes on the climate system. To highlight the AMOC-induced SO response rather than intrinsic variability, all results shown are ensemble means.

Several observational and reanalysis datasets are used to evaluate the model results. We use an extended reconstructed SST (ERSST) data set on a $2^{o}\times2^{o}$ grid from 1854 to 2013 (Smith and Reynolds 2004). We use the Hadley Centre Sea Ice and sea surface temperature data set (HadISST), available on a $1^{o}\times1^{o}$ grid from 1870 to 2013 (Rayner et al. 2003). We use the monthly objectively analyzed subsurface temperature data set (Ishii et al. 2005) from 1945 to 2013, which has a horizontal $1^{o}\times1^{o}$ grid, with 23 layers in the upper 1500m. We also use the atmospheric reanalysis product for the 20^{th} century, designated as 20CRv2. The reanalysis output extends from 1871 to 2010, with output available at 2° spatial resolution (Compo et al. 2011). Finally, we use the ECDA reanalysis dataset (Zhang et al. 2007) that is based on an ensemble adjustment Kalman filter applied to the fully coupled GFDL CM2.1 model, in which the atmosphere is constrained by the NCEP atmospheric analysis and the ocean assimilates observations of SST from satellite and temperature and salinity from the World Ocean Database 2009. The ECDA reanalysis has the same horizontal and vertical resolutions with the GFDL CM2.1 and has a time period from 1961 to 2013.

3. Simulated SO response to the multidecadal AMOC variations induced by the NAO

Before investigating the SO response to the multidecadal AMOC change, we define some indices to represent typical circulations over the Atlantic and SO. Fig. 2a shows the latitude-depth section of the long term mean streamfunction in the fully coupled control run. Note that the streamfunction north of 32°S is integrated in the Atlantic Ocean, while south of 32°S it denotes the global streamfunction. The AMOC is characterized by a clockwise circulation, with a northward flow in the upper 1500-m and a southward flow below. Consistent with previous studies (e.g. Schmitz 1996; Swingedouw et al. 2009), the isopycnal 27.6 kg/m^3 (white line in Fig. 2a) approximately corresponds to the limit between the upper and lower branches of the AMOC. Here, we define the AMOC index as the maximum streamfunction value in 20°N-60°N band and below 500-m. The depth limit is used to exclude the shallow subtropical cell (STC) in the upper layer. In the control run, the AMOC maximum, which is located near 49.5°N and 1400-m depth, is about 26 Sv. In the SO, there is a strong clockwise MOC around the Antarctic circumpolar current (ACC) region (~40°S-60°S). In contrast to the buoyancy-driven AMOC, this meridional cell is mainly wind-driven. The prevailing westerly over the ACC region induces a northward Ekman transport in the surface, leading to a water divergence (convergence) south (north) of westerly. Due to mass conservation, the downwelling formatted in the convergence region tends to move southward, then upwells to the surface to compensate local water divergence and eventually generates a clockwise MOC named as Deacon Cell. The strength of Deacon Cell here is well represented by the maximum streamfunction in the 40°S-60°S band. The long term mean Deacon Cell in

194 GFDL CM2.1 control run is about 30 Sv. The streamfunction value south of 60°S is
195 negative (Fig. 2a), which represents a counterclockwise cell and mainly reflects the
196 AABW formation. Here, we use the absolute value of the minimum streamfunction
197 south of 60°S from surface to the bottom of the ocean to represent the strength of
198 AABW. The AABW value is about 10 Sv in GFDL model using this definition.

199 We show in Fig. 3 the AMOC, AABW and Deacon Cell responses to the
200 idealized multidecadal NAO forcing. To focus on multidecadal variability, we also
201 display the 30-yr low pass filtered indexes. Fig. 3a exhibits that the low-passed
202 AMOC index is simultaneously in phase with the NAO forcing at a time scale of 100
203 years, with a positive NAO corresponds to a spin up of the AMOC and vice versa.
204 Physically, the positive (negative) NAO-related heat flux tends to extract (input) heat
205 from (to) the ocean, thereby cooling (warming) and increasing (decreasing) the
206 density of the upper ocean, and in turn leading to a strengthened (weakened) AMOC
207 (e.g. Delworth and Dixon 2000; Lohmann et al. 2009). Note that the response time of
208 the AMOC to the NAO forcing is around a decade or less (Lohmann et al. 2009;
209 Delworth and Zeng 2015), and this adjustment time is much shorter than the forcing
210 period (100-yr). That means the AMOC is fully adjusted and goes into an equilibrium
211 state in each phase of the forcing, therefore, there is no obvious time lag between the
212 AMOC index and NAO forcing. In response to one standard deviation of observed
213 NAO variability, the multidecadal AMOC changes ~4 Sv (peak to peak) (Fig. 3a),
214 which accounts for ~12% (peak to peak) of the long term mean AMOC (Fig. 3b).

215 We now turn our attention to the SO. The deepest impression from Fig. 3a is that

the AABW cell varies out of phase with the AMOC index on multidecadal time scales, with a spin up of AMOC corresponding to a weakened AABW formation and vice versa. We note that the real magnitude change of AABW cell (~1.5 Sv, peak to peak) is smaller than the AMOC response (~4 Sv, peak to peak, Fig. 3a). However, the percentage change of AABW cell is comparable to, sometime even higher than, the AMOC change (Fig. 3b). We can also characterize this anti-correlated relationship between the AMOC and AABW cell by the mixed layer depth change. As shown in Fig. 3c, the deepened (shoaled) mixed layer depth over the North Atlantic deep convection region (Labrador sea, Irminger sea and south Greenland) associated with a stronger (weaker) than normal AMOC coincides with a shoaled (deepened) mixed layer depth in the Weddell sea. This ocean bipolar seesaw phenomenon in the current climate is similar to the work of Broecker (1998, 2000) in the context of the paleoclimatic record. The green lines shown in Fig. 3a and b are the wind-driven Deacon Cell response to a 100-yr periodic NAO forcing. The Deacon Cell response is positively correlated with the AMOC change with a lag of several decades. This indicates that the westerly wind over the SO tends to strengthen (weaken) as the AMOC accelerates (decelerates).

The isopycnal depth variation is useful in illustrating the density driven circulation (AMOC and AABW cell) response to NAO fluxes. We plot the time evolution of Atlantic zonal mean 27.6 kg/m^3 isopycnal depth anomaly at various latitudes to further show how the AMOC signal propagates and how the AABW cell responds in meridional direction (Fig. 4). In the NAO forcing region, the spin up

238 (down) of AMOC corresponds to a shoaling (deepening) of the 27.6 kg/m^3 isopycnal
239 (Fig. 3a versus Fig. 4). This is because: The increased (decreased) density as the
240 AMOC strengthens (weakens) in the whole column of North Atlantic favors an
241 increase (a decrease) of the NADW production. This deep water mass is replaced by
242 heavier (lighter) water in the surface layers of the ocean, which shoals (deepens) the
243 27.6 kg/m^3 isopycnal. The shoaled (deepened) isopycnal in the northern high latitudes
244 then propagates southward in two different speeds separated by 35^{o}N. The
245 propagation speed north of 35^{o}N is very slow, while in 35^{o}N-35^{o}S band the speed is
246 very fast that almost varies simultaneously in different latitudes. This latitudinal
247 dependence of isopycnal propagation speed is an interactive product of external
248 forced period and internal advective/wave speed inside the Atlantic Ocean. As
249 suggested by Zhang (2010), the interior advection speed determines the AMOC
250 propagation time north of 35^{o}N. Note that this is the region where it is forced by a
251 strong external forcing with a period of 100-yr that is much longer than the internal
252 advective time inside the Atlantic Ocean. The coupled effect of external forcing and
253 internal advection speed in turn generates the slow propagation speed of 27.6 kg/m^3
254 isopycnal north of 35^{o}N. From the equator to 35^{o}N, the propagation speed is mainly
255 determined by the fast Kelvin wave along the western boundary (Zhang 2010), hence,
256 the 27.6 kg/m^3 isopycnal depth at various latitudes in this band are almost in phase. In
257 the equator, the Kelvin wave moves eastward quickly and then propagates southward
258 to the SH along the eastern boundary. In the eastern boundary, the isopycnal anomaly
259 also spreads westward by the Rossby wave with a slower speed at higher latitudes

than at lower latitudes (e.g. Johnson and Marshall 2002; Zhang 2010). Therefore, the propagation speed of 27.6 kg/m^3 isopycnal depth from equator to 35^{o}S is affected by both Kelvin and Rossby wave speeds.

The 27.6 kg/m^3 isopycnal depth change south of 40^{o}S is totally antisymmetric to that in the Northern Hemisphere (NH), with a shoaling depth in the North Atlantic coinciding with a deepening of isopycnal depth in the Weddell sea and vice versa. The isopycnal deepening (shoaling) implies that the AABW formation decreases (enhances), which is largely due to the decreased (increased) density over the Weddell Sea (not shown). Similar to the North Atlantic, the high latitudinal isopycnal depth anomaly in the SH gradually propagates northward, with a forced slow advection speed south of 57^{o}S and a fast Kelvin wave speed north of 57^{o}S along the western boundary. Note that the isopycnal depth anomaly over the Weddell Sea (south of 70^{o}S) lags that over the South Greenland (north of 45^{o}N) by about two decades. This implies that the AABW cell passively responds to the AMOC change or its associated climate impacts. Moreover, the isopycnal depth propagation within the SO advection band (south of 57^{o}S) takes a shorter time than that in the North Atlantic (north of 35^{o}N) because of the shorter advection distance in the SH compared to NH.

In agreement with the isopycnal depth propagation, the AMOC index shows a strong latitudinal dependence. As presented in Fig. 5, the high latitudinal AMOC index (red line) leads the relatively low latitudinal AMOC index (green line) by several years. The anomalous AMOC finally leads to significant SST anomalies over the North Atlantic due to the anomalous northward heat transport, characterized by a

282 warm SST anomaly over the North Atlantic as the AMOC strengthens and vice versa
283 (Fig. 5a). A close examination finds that the North Atlantic SST lags the extratropical
284 AMOC index by several years. This lag is primarily due to the slow adjustment of
285 ocean.

286 Similar to the AMOC, the AABW variations are finally reflected in the SO
287 temperature. Fig. 5b exhibits that the AABW cell varies in phase with the SO SST but
288 with a lead of several years. Again, this lead-lag is attributed to the ocean adjustment
289 time. Given that the mean state of SO subsurface ocean is warmer than the surface,
290 the stronger than normal AABW cell is in favor of entraining more subsurface warm
291 water to the surface, which in turn generates a warm SST anomaly in the surface and a
292 cold SST in the subsurface and vice versa. This explanation is further confirmed by
293 the regressed zonal mean temperature pattern upon the SO SST index (Fig. 6a) that
294 shows an obvious temperature dipole in the SO. Note that the entire NH in Fig. 6a is
295 featured by typical AMOC fingerprints such as the tropical North Atlantic
296 surface-subsurface temperature dipole (e.g. Zhang 2010; Wang and Zhang 2012),
297 indicating a strong linkage between the AMOC and SO on multidecadal time scales.
298 Due to the out of phase relationship between the AMOC and AABW cell, the SST
299 anomalies in the North Atlantic and SO are strongly anticorrelated (Fig. 5 and Fig. 6a).
300 This inter-hemispheric dipole SST structure is more clearly seen from the regressed
301 global SST pattern upon the North Atlantic SST index (Fig. 6b).

302 The SO SST anomalies could further feedback to the overlying atmosphere. We
303 perform two sensitivity experiments. The first run is control restoring experiment in

304 which we restore the model output SST at every step to the climatological SST
305 seasonal cycle in control simulation over the SO (50°S-90°S, 80°E-80°W), while the
306 ocean and atmosphere are fully active elsewhere. The other experiment is the same as
307 the first run, but with the SST in the SO restoring to an SST field that is the sum of the
308 seasonal cycle from the control simulation plus the SST anomaly south of 50°S
309 derived from the regression pattern (Fig. 6b). Both runs are integrated for 50 years
310 and the last 40 years differences are taken as the response. A 10-member ensemble run
311 is performed with each experiment starting from an equilibrium state of a long fully
312 coupled control simulation, and the ensemble-mean response is shown. In response to
313 a cold SST anomaly in the SO, the sea level pressure (SLP) anomaly is characterized
314 by a positive phase of Southern Annular Mode (SAM) and strengthened westerly
315 winds (Fig. 6c). Note that the magnitude of SLP response is much smaller than the
316 simultaneously regressed SLP anomaly which mainly reflects the atmosphere forcing
317 of ocean (Fig. 6b versus Fig. 6c), indicating a weak SST feedback over the SO. The
318 enhanced westerly can amplify the initial SO cold SST anomaly via increased latent
319 heat loss and northward Ekman transport, which in turn generates a local weak
320 positive air-sea feedback. The enhanced westerly also leads to a spin up of the Deacon
321 cell after the adjustments of ocean (Fig. 5b).

322 We show in Fig. 7 the SO sea ice response to the NAO forcing at a time scale of
323 100 year (Fig. 7). Generally speaking, the annually SO sea ice is increased (decreased)
324 when the SO SST becomes cool (warm) (Fig. 7a), particularly in the Ross and
325 Weddell seas where the deep water forms. Here, local ocean temperature is the

dominant factor to determine sea ice change. The sea ice response is also somehow affected by the surface wind during the austral winter when the surface wind is strongest throughout the year. In the austral winter, the low pressure system over the Amundsen Sea is extremely low, favoring a warm air advection from subtropics to the Antarctic Peninsula region and a cold air advection from polar Antarctic to the Ross and Amundsen seas (Fig. 7b) and vice versa. This anomalous warm/cold air advection eventually drives a weak sea ice dipole distribution displayed in Fig. 7b.

4. Physical mechanisms controlling the SO response to the multidecadal AMOC variations

In this section, we attempt to address what mechanisms control the ocean bipolar seesaw described above, particularly what processes determine the SO response. We first examine the possible contributors in the 100-yr periodic NAO forcing experiment. Then we use a "switch on" experiment, in which we suddenly turn on and maintain an anomalous positive NAO flux forcing whose amplitude corresponds to one standard deviation of the NAO time series, to further confirm our hypothesis.

a. Implications from the 100-yr periodic NAO forcing experiment

Show in Fig. 8a are the regressed surface wind stress and wind stress curl anomalies at each grid point versus the area averaged North Atlantic SST time series. The westerly wind over the SO is characterized by a strengthening (weakening) and poleward (northward) shift as the North Atlantic warms (cools) generated by the accelerated (decelerated) AMOC. These results suggest that the SO westerly wind anomaly is likely to be a remote response to the anomalous North Atlantic SST

induced by the AMOC via atmosphere bridges. This trans-hemispheric atmosphere teleconnection will be verified later.

Consistent with the wind response, the wind stress curl anomaly south of 40°S shows a dipole structure with broad positive values in the north and negative values in the south (Fig. 8a). The positive (negative) wind stress curl over the South Atlantic (40°-60°S) associated with a spin up (down) of AMOC favors a deepening (shoaling) of the isopycnal depth. By overlapping this wind-driven pycnocline depth anomaly, the 27.6 kg/m^3 isopycnal depth shows a much stronger signal over the 40°-60°S band than that in the high latitudinal deep convection region (Weddell sea) where the buoyancy forcing is dominant (Fig. 4).

The westerly wind over the SO further induces surface net heat flux anomalies over the Weddell Sea where the AABW forms. Fig. 8b shows that a strengthening and poleward shifted westerly is accompanied with a net heat flux input into the Weddell Sea and vice versa. We note that the long term mean wind stress is a prevailing easterly over the Weddell Sea (Fig. 2c). The anomalous westerly (easterly) wind associated with an accelerated (a decelerated) AMOC weakens (strengthens) the wind speed over the Weddell Sea, reduces (enhances) the turbulent heat loss and therefore warms the ocean. We also show in Fig. 8c the area averaged heat flux over the Weddell Sea and the AABW time series. The net heat flux anomaly contributed mainly from the turbulent heat flux (latent and sensible fluxes) fluctuates almost out of phase with the AABW cell on multidecadal time scales, with a heat flux warming the ocean coinciding with a decelerated AABW Cell and vice versus. This implies that

370 the multidecadal AABW cell fluctuation is likely driven by the local heat flux induced
371 by the westerly anomaly. As discussed above, the anomalous westerly is likely
372 triggered by the North Atlantic SST associated with the AMOC variation via
373 atmosphere teleconnection.

374 **b. Response to "switch-on" of NAO forcing**

375 We perform a "switch-on" experiment to verify our hypothesis mentioned above.
376 In this "switch-on" experiment, we suddenly turn on the extra positive NAO heat flux
377 forcing, at a random point in the control simulation, and leave these fluxes on with
378 constant amplitude corresponding to one standard deviation of the observed NAO
379 time series. This experiment allows us to understand the spin up process of the
380 climate system in response to an instantaneous imposition of the extra positive NAO
381 heat fluxes. We conduct 10-member ensembles of this "switch-on" setup and each
382 ensemble member integrates forward for 150-yr. The ensemble mean difference
383 between the "switch-on" experiment and fully coupled control run is taken as the
384 response.

385 Shown in Fig. 9a is the time series of AMOC and AABW cell responses to the
386 NAO-related flux forcing. The simulated AMOC adjusts over one decade, increasing
387 in amplitude by several Sverdrups (Sv). This positive AMOC anomaly is largely
388 associated with increased density in the deep convection region due to increased latent
389 heat loss during the positive phase of the NAO (e.g. Delworth et al. 2002; Delworth
390 and Zeng 2015). Note that the AMOC index oscillates with a period around 10-28
391 years; although the NAO flux forcing is constant. This is because the characteristic

time scale of these oscillations is modulated by the internal variability in GFDL CM2.1 (Delworth and Zeng 2015). As the AMOC increase becomes stable, the AABW cell gradually weakens. The AABW index is dominant by negative anomalies after about 50 year. This AABW cell decreasing is also clearly seen from the last 100 year (year 51-150) averaged global meridional overturning streamfunction (GMOC) response (Fig. 10a). The GMOC anomaly exhibits a broad positive value in the upper 4000m in all latitudes, indicating a strengthened AMOC and a weakened AABW cell. Due to these cell changes, the temperature anomaly features a dipole structure over both the North Atlantic and SO but with an opposite sign (Fig. 10a).

We then examine what processes determine the AABW decreasing? As implied by the 100-yr periodic NAO forcing experiment, we first investigate the surface heat flux over the Weddell Sea (Fig. 9b). A close inspection finds that the surface net heat flux is dominant by positive anomalies after about 30 years when the AMOC is fully adjusted and the North Atlantic Ocean displays a strong warming (Fig. 10b). It is worth noting that the positive heat flux anomaly leads the AABW cell decreasing by several years, indicating that the AABW anomaly is driven by, rather than initially induces, the surface heat flux (Fig. 9b). Further decomposition reveals that this anomalous surface net heat flux mainly arises from its turbulent heat flux (latent plus sensible flux), while the contribution from radiative forcing is negligible (Fig. 9c). We also show in Fig. 10b and Fig. 10c the time averaged (year 31-50) surface net heat flux and wind stress responses to the constant NAO forcing. The surface net heat flux over the Weddell Sea tends to warm the ocean; this is consistent with an anomalous

414 anticlockwise wind in the extratropical South Atlantic, with a weakening of the long
415 term mean easterly over the Weddell Sea (Fig. 10c versus Fig. 2c). The anomalous
416 anticlockwise wind stress around 40°-60°S band corresponds to a positive wind stress
417 curl (Fig. 10c), which favors a deepening of the isopycnal over the extratropical South
418 Atlantic.

419 We show in Fig. 11 the time evolution of meridional averaged density anomaly in
420 response to a suddenly imposed NAO forcing. In the first decade, the North Atlantic
421 density increases in both surface and subsurface; this is largely associated with the
422 strengthening of AMOC (Fig. 11a) due to the positive NAO flux forcing. The SO
423 shows no obvious response at this time. As the time integrates forward (year 11-50),
424 the positive density anomaly over the North Atlantic grows and gradually extends
425 southward to the South Atlantic in the subsurface (Fig. 11b-e). This southward
426 penetration is again related to the acceleration of AMOC. In sharp contrast, there is a
427 density decrease over the SO, which is mainly confined within 40°S-60°S band (Fig.
428 11b-e). This negative density anomaly is attributed to the positive wind stress curl
429 shown in Fig. 10c. The positive wind stress curl over the SH favors a surface water
430 convergence, a deepened isopycnal depth, an increased upper ocean heat content and
431 SST (Fig. 10b), and thus a decreased density in a whole column. In the south of 60°S,
432 the density shows a slight increase in the subsurface from year 11 to 50 (Fig. 11b-e).
433 There is a very weak decrease of density in the surface after year 30 (Fig. 11d-e). At
434 year 51-60, the negative density anomaly south of 60°S extends to the upper ocean
435 (Fig. 11f). These density decreases primarily arise from the anomalous surface heating

436 as a result of decreased wind speed over the Weddell Sea (Fig. 10b and c). The
437 decreased density over the SO further grows and progressively penetrates into the
438 deep ocean (Fig. 11g-j), which in turn leads to a weakened AABW cell.

439 The above suggest that the AABW weakening in response to a strengthened
440 AMOC is largely associated with the surface heat flux heating over the Weddell Sea
441 as a result of decreased wind speed. Fig. 10b and c further show that this wind speed
442 change over the SO corresponds to a SST warming over the North Atlantic. In the
443 next, we will use sensitivity experiments to prove this trans-hemispheric atmosphere
444 bridge.

445 We conduct two parallel experiments to examine whether the AMOC-induced
446 North Atlantic SST anomaly are responsible for driving the SO variability. In the first
447 run, we restore the SSTs in the North Atlantic (0^{o}N-70^{o}N, coast to coast) to their
448 climatological seasonal cycle with a restoring time scale of 5 days, while elsewhere
449 the ocean and atmosphere are fully coupled. The second run is configured as the same
450 as the first run, except that the SSTs in the North Atlantic are restored to their
451 climatological seasonal cycle plus the AMOC-induced North Atlantic SST (0^{o}N-70^{o}N)
452 anomaly shown in Fig. 10b. The difference between the first run and the second run is
453 taken as the climate response to the anomalous North Atlantic SST anomaly and
454 named as “Restore_NASST”. A 10-member ensemble experiment is performed with
455 each experiment starting from widely separated states of the model’s control
456 simulation. Each member runs for 50 years and the last 40-year ensemble means are
457 taken as the equilibrium response.

458 We show in Fig. 12a the SST and SLP responses in experiment “Restore_NASST”.
459 The SO generally experiences a cold SST anomaly. The overlying atmosphere is
460 characterized by a positive phase of SAM, with a high pressure cap surrounded the
461 polar region and a low pressure in the mid-latitude. This anomalous SLP response
462 corresponds to a strengthening and southward shift of the westerly, which could
463 generate a weakened AABW cell and subsequent SST cooling. We also note that the
464 high SLP over the extratropical South Atlantic (around 40^{o}S-60^{o}S) can induce a
465 surface water convergence, which is accompanied with a deepening of the subsurface
466 isopycnal depth, an increased upper ocean heat content and a warm SST anomaly.
467 To elucidate how the North Atlantic SST warming drives the SO westerly
468 anomaly, we show the vertical structures of global air temperature changes (Fig. 12b).
469 Significant, broad warming is found in the NH from the surface to the upper
470 atmosphere. There is an exception in the low stratosphere, where cooling occurs. The
471 NH warming tends to penetrate south upward into the tropical upper troposphere. This
472 amplified tropical upper tropospheric warming is largely due to increased latent heat
473 release through enhanced moist convection. In the SH, a weak warming is exhibited
474 in the low and middle troposphere at middle and high latitudes, whereas a broad
475 cooling appears above 350 hPa at high latitudes. These temperature features in the SH
476 suggests an increased static stability in the SH mid-latitudes and an increased
477 equator-to-pole temperature gradient in the SH upper troposphere and lower
478 stratosphere, which could push the westerly jet poleward and strengthen westerly
479 winds. Here, the atmosphere bridge from the North Atlantic to the SO is consistent

480 with Li et al. (2015) and Wang et al. (2015).

481 **5. Is the recent SO variation tied to AMOC change?**

482 Over the past few years, most regions in the earth have shown considerable
483 temperature increase in response to greenhouse gas emissions (e.g. Vecchi et al. 2008;
484 Zhang et al. 2011). However, the SO has cooled. Fig. 13 exhibits the area averaged
485 SO SST anomaly from 1961 to 2013 in four independent datasets including HadISST,
486 ERSST, Ishii and ECDA reanalysis. The extratropical North Atlantic SST time series
487 is also displayed to do comparison. All data show a consistent decreasing trend of SO
488 SST after 1979 especially after 2000 when the cooling SST predominates, while SST
489 anomalies over the extratropical North Atlantic exhibit a significant increase. A close
490 inspection reveals that the extratropical North Atlantic SST varies in phase with the
491 AMO index, indicating that the internal variability may play an important role. Here,
492 we use the signal-to-noise maximizing Empirical Orthogonal Function (S/N EOF)
493 (e.g. Ting et al. 2009) to separate the internal variability and external forced response
494 in the SST field. Given that the ECDA reanalysis is based on GFDL CM2.1, we
495 choose the first S/N EOF mode derived from ten members of GFDL CM2.1 historical
496 run as the forced SST response in four datasets for consistency. The forced SST signal
497 is then derived by projecting the area averaged SST anomaly onto the first principal
498 component (PC1). The residual between the original SST time series and the forced
499 SST signal is referred to as the internal variability, which is also shown in Fig. 13. It
500 can be seen that the original and internal variability of extratropical North Atlantic
501 time series are overlapped together. This implies that the extratropical North Atlantic

SST variability is completely driven by the internal variability over the North Atlantic where the AMOC variation dominates. The internal variability of SO SST has the same sign with the original time series but has a much larger amplitude, particularly after 2000, indicating that the external forcing tends to offset but is not a primary factor to determine the SO SST. Moreover, the internal variability of SO SST is negatively correlated with the extratropical North Atlantic SST (or the AMO index), with a warming anomaly in period 1965-1995 and a significant cooling after 1995. This out of phase relationship shares great similarities with the bipolar SST seesaw induced by the multidecadal AMOC variations (Fig. 6), suggesting that the AMOC may play an important role in the recent SO SST change.

To clearly show the spatial structure of SO SST change, we calculate a SST field difference between period 1996-2013 and 1979-1995, as displayed in Fig. 14a-d. Consistent with area averaged anomalies, the SST features a broad cooling over the SO, with large values over the Pacific and Atlantic basins (Fig. 13 versus Fig. 14). The atmosphere exhibits a low pressure overlying the cooling SST (Fig. 14a, d), indicating a poleward shift and enhancement of the westerly. Note that the SST outside the SO region also shows significant changes, which resembles the positive phase of AMO (Fig. 14a-d). As discussed in section 4, the Atlantic (0^{o}-70^{o}N) SST warming favors producing a low pressure system over the SO via fast atmosphere bridges. This implies that the recent SO SST change may be attributed, at least partially, to the North Atlantic SST where the internal AMOC variability cannot be negligible.

In contrast to the surface cooling, the subsurface SO shows a significant warming in recent decades (Fig. 15). Both the Ishii data and ECDA reanalysis exhibit an accelerated column averaged warming in the SO subsurface after 2000, albeit with some differences on interannual time scale (Fig. 15a, b). These inconsistencies may arise from the paucity of observations in the SO as well as the model uncertainty. The zonal mean SO temperature difference between period 1996-2013 and 1979-2005 further verifies this surface-subsurface temperature dipole (Fig. 15c, d). This vertical temperature structure in the SO implies that the AABW formation is weakened in the past few years. To investigate this hypothesis, we plot the AABW, AMOC and Deacon Cell time series in ECDA reanalysis. Here, the MOC definition is based on streamfunction (Fig. 2b), which is the same as that in GFDL CM2.1 model. As presented in Fig. 16a, the AABW cell has a multidecadal fluctuation, with a weakened value after 1990. On the contrary, the AMOC and Deacon Cell are strengthened in the recent two decades. Moreover, these MOC changes are largely attributed to the internal variability (Fig. 16b, c). Fig. 16b shows the ensemble mean MOC time series in GFDL historical run, which mainly reflects the effect of external forcing. As expected, both the AMOC and AABW cell are weakened due to the greenhouse gas induced anomalous heating and freshening (e.g. Cheng et al. 2013; Ma and Wu 2011). The Deacon cell is strengthened under the global warming scenario, which is largely associated with the enhanced westerly as a result of Ozone increase (e.g. Turner et al. 2009). After removing the external forced MOC change, the residual MOC variability still has the same sign with the original time series (Fig. 16a versus Fig. 16c),

546 indicating a predominant role of internal variability. The SO MOC changes in recent
547 decades are in agreement with their response to the multidecadal AMOC variations
548 (Fig. 3a). This, again, suggests the potential possibility of AMOC influence on the SO
549 via fast atmosphere bridges and subsequent ocean adjustments.

550 The sea ice change in recent years is strongly coupled with the SST and surface
551 wind. Fig. 17 shows the sea ice difference between period 1996-2013 and 1979-1995
552 in different seasons. Consistent with Li et al. (2014), the sea ice change during the
553 austral winter (JJA) is characterized by a dipole distribution, with a sea ice increase in
554 the Ross sea, and a broad sea ice decrease in the Amundsen-Bellingshausen-Weddell
555 seas (Fig. 17a). This sea ice dipole is primarily attributed to the Amundsen Sea low
556 induced onshore/offshore air advection as discussed in section 3. During the austral
557 summer (DJF), the sea ice shows a broad increase corresponding to a SST cooling
558 (Fig. 17b). In this season, the ocean temperature becomes a dominant factor to
559 determine the sea ice distribution. The annual mean sea ice change mainly follows the
560 austral winter pattern, albeit with a small amplitude. The dynamical mechanism
561 controlling the sea ice distribution in recent years is generally in agreement with the
562 sea ice response in Fig. 9, which, again, suggests a potential linkage with the AMOC.

563 Our observational evidences suggest that the SO change has a large possibility to
564 be influenced by the AMOC. This implies that attributing the recent SO variability
565 should take into consideration not only the local process but also the remote AMOC
566 forcing. While emphasizing the potential role of AMOC in the SO change, we do not
567 wish to down play the potential importance of local circulation and feedbacks in

causing the large SO variations such as the internal SO variability independent of AMOC (e.g. Latif et al. 2013).

6. Discussion and Summary

The impact of multidecadal AMOC variations on the SO is studied in the present paper using the fully coupled GFDL CM2.1 model. It is found that the AMOC can influence the SO via fast atmosphere bridges and subsequent ocean adjustments. A stronger than normal AMOC induces an anomalous warm SST over the North Atlantic, which favors an increased equator-to-pole temperature gradient in the Southern Hemisphere (SH) upper troposphere and lower stratosphere due to an amplified tropical upper tropospheric warming as a result of increased latent heat release. This eventually strengthens and pushes the westerly jet poleward. Here, the atmosphere bridge from the North Atlantic to the SO is consistent with Li et al. (2014) and Wang et al. (2015).

The enhanced and poleward shifted westerly wind over the SO cools the SST by the anomalous norward Ekman transport on one hand and weakens the AABW cell through anomalous heat flux. The latter is because the poleward shifted westerly wind decreases the long term mean easterly over the Weddell Sea, reducing the turbulent heat flux loss, decreasing the sea water density and therefore leading to a weakened AABW cell. In the mean state the subsurface is warmer than the surface in the region of the AABW. Therefore, the spin down of AABW cell drives a surface-subsurface temperature dipole in the SO, with a warming anomaly in the subsurface and a cooling anomaly at the surface that corresponds to an increase of Antarctic sea ice.

590 The SO SST cooling can further feedback to the atmosphere, modestly increasing the
591 westerly winds thereforestrengthening the Deacon cell. The westerly wind response
592 further amplifies the initial SO surface cooling by the enhanced latent heat loss and
593 anomalous northward Ekman transport. Therefore, there is a weak positive air-sea
594 feedback in the SO. The opposite is also true for a weaker than normal AMOC.

595 The sensitivity of SO response to periodic NAO forcing on time scales ranging
596 from 20 to 200 years is accessed. We see that the model AABW has very little
597 response to forcing at time scales shorter than five decades or so (not shown). The
598 adjustment processes by which the AABW responds to the AMOC and the AMOC
599 responds to the NAO take of order five decades, so that forcing on shorter timescales
600 is not able to significantly influence the AABW. At longer timescales the AABW
601 varies largely in phase with AMOC and NAO forcing, although exhibiting some
602 preference for forcing close to the dominant timescale of SO internal variability
603 (approximately 50-110 years for the GFDL CM2.1 model) (not shown).

604 The dynamical linkages between the AMOC and SO have some implications for
605 the recent observed SO change. The SO SST depicts pronounced multidecadal
606 variations during the instrumental period. During the recent two decades with the
607 advent of satellite, the observations consistently show a cooling SST trend over the
608 SO, while the North Atlantic exhibits a significant warming trend. Moreover, the
609 subsurface SO temperature features a warm anomaly. This surface-subsurface dipole
610 temperature structure implies that the AABW formation is weakened. ECDA
611 reanalysis confirms that the AABW cell does weaken in the past few years, which

coincides with a strengthened AMOC. We hypothesize that the remarkable SO SST cooling during the recent decades can be attributed, at least partly, to the AMOC change. We need to keep in mind that the observed multidecadal/trend pattern might be a superposition of several internal modes and externally forced variability. The good correspondence of the observed changes with the model patterns may be thus partly coincidental. Furthermore, the methods used to separate the internal and external variability, such as the S/N EOF used in current paper, are still under debate. More and more direct ocean observation, particularly subsurface observations over the far SO, are needed to better assess the model variability and verify the existence of bipolar ocean seesaw in the real world. Comparison of the AMOC influence on the SO in the GFDL model with that simulated by other climate models will also be helpful.

Acknowledgment:

The authors would like to thank Dr. Fanrong Zeng for her great help in running part of the model experiments.

629 Reference:

630 Altabet MA, Higginson MJ, Murray DW (2002) The effect of millennial-scale
631 changes in Arabian Sea denitrification on atmospheric CO2. Nature 415: 159–
632 162

633 Blunier T, Brook EJ (2001) Timing of millennial-scale climate change in Antarctica
634 and Greenland during the last glacial period. Science 291: 109–112

635 Bryden H, Longworth HR, Cunningham SA (2005) Slowing of the Atlantic
636 meridional overturning circulation at 25°N, Nature 438: 655–657

637 Broecker WS (1998) Paleocean circulation during the last deglaciation: A bipolar
638 seesaw? Paleoceanography 13: 119–121

639 Broecker WS (2000) Was a change in thermohaline circulation responsible for the
640 Little Ice Age? Proc Natl Acad Sci 97: 1339–1342

641 Black DE, Peterson LC, Overpack JT, Kaplan A, Evans MN, Kshgarian MK (1999)
642 Eight centuries of North Atlantic ocean atmosphere variability. Science 286:
643 1709–1713

644 Cheng W, Chiang JCH, Zhang D (2013) Atlantic Meridional Overturning Circulation
645 (AMOC) in CMIP5 Models: RCP and Historical Simulations. J Climate 26:
646 7187–7197

647 Crowley TJ (1992) North Atlantic deep water cools the Southern Hemisphere.
648 Paleoceanography 7: 489–497

649 Compo GP, Whitaker JS, Sardeshmukh PD, Matsui N, Allan BJ, Yin X, Gleason BE,
650 Vose RS, Rutledge G (2011) The twentieth century reanalysis project. Quarterly

651 J Roy Meteorol Soc 137: 1–28
652 Delworth TL, Manabe S, Stouffer RJ (1993) Interdecadal variations of the
653 thermohaline circulation in a coupled ocean-atmosphere model. Journal of
654 Climate 6: 1993-2011
655 Delworth TL, Mann ME (2000) Observed and simulated multidecadal variability in
656 the Northern Hemisphere. Climate Dynamics 16: 661-676
657 Delworth TL, Dixon KW (2000) Implications of the recent trend in the Arctic/North
658 Atlantic Oscillation for the North Atlantic Thermohaline Circulation. Journal of
659 Climate 13: 3721-3727
660 Delworth TL et al (2006) GFDL's CM2 Global Coupled Climate Models. Part I:
661 Formulation and Simulation Characteristics. J Climate 19: 643–674
662 Delworth TL et al (2008) The potential for abrupt change in the Atlantic Meridional
663 Overturning Circulation In Abrupt Climate Change: Final Report, Synthesis &
664 Assessment Product 3.4, CSSP, Reston, VA, U.S. Geological Survey, 258-359
665 Delworth TL, Zeng F (2012) Multicentennial variability of the Atlantic Meridional
666 Overturning Circulation and its climatic influence in a 4000 year simulation of
667 the GFDL CM2.1 climate model. Geophysical Research Letters 39, L13702,
668 doi:10.1029/2012GL052107
669 Delworth TL, Zeng F (2015) The impact of the North Atlantic Oscillation on climate
670 through its influence on the Atlantic Meridional Overturning Circulation.
671 Submitted to Journal of climate

672 Dong BW, Sutton RT (2002) Adjustment of the coupled ocean–atmosphere system to
673 a sudden change in the thermohaline circulation. Geophys Res Lett 29: 1728
674 Dong BW, Sutton R T (2007) Enhancement of ENSO variability by a weakened
675 Atlantic thermohaline circulation in a coupled GCM. J Climate 20: 4920–4939
676 Folland CK, Parker DE, Kates FE (1984) Worldwide marine temperature fluctuations
677 1856–1981. Nature 310: 670–673
678 Gray WM, Sheaffer JD, Landsea CW (1997) Climate trends associated with
679 multidecadal variability of Atlantic hurricane activity, in Hurricanes: Climate
680 and Socioeconomic Impacts, edited by H. F. Diaz and R. S. Pulwarty, pp. 15–53,
681 Springer, New York.
682 Hurrell JW (1995) Decadal trendsin the North Atlantic Oscillation region
683 temperatures and precipitation. Science 269: 676–679
684 Ishii M, Kimoto M, Sakamoto K, Iwasaki SI (2006) Steric sea level changes estimated
685 from historical ocean subsurface temperature and salinity analyses. J
686 Oceanography 62: 155-170
687 Johnson HL, Marshall DP (2002) A theory for the surface Atlantic response to
688 thermohaline variability. J Phys Oceanogr 32: 1121–1132
689 Knight JR, Allan RJ, Folland CK, Vellinga M, Mann ME (2005) A signature of
690 persistent natural thermohaline circulation cycles in observed climate. Geophys
691 Res Lett 32: L20708, doi:10.1029/2005GL024233
692 Latif M, Martin T, Park W (2013) Southern Ocean Sector Centennial Climate
693 Variability and Recent Decadal Trends. J Climate 26: 7767–7782

694 Li X, Holland DM, Gerber EP, Yoo C (2014) Impacts of the north and tropical
695 Atlantic Ocean on the Antarctic Peninsula and sea ice. Nature 505: 538-542
696 Lohmann K, Drange H, Bentsen M (2009) Response of the North Atlantic subpolar
697 gyre to persistent North Atlantic oscillation like forcing. Climate Dyn 32: 273–
698 285
699 Ma H, Wu L (2011) Global Teleconnections in Response to Freshening over the
700 Antarctic Ocean. J Climate 24: 1071–1088
701 Martin T, Park W, Latif M (2013) Multi-centennial variability controlled by Southern
702 Ocean convection in the Kiel Climate Model. Climate Dyn 40: 2005–2022
703 Peterson LC, Haug GH, Hughen KA, Rohl U (2000), Rapid changes in the
704 hydrological cycle of the tropical Atlantic during the last glacial. Science 290:
705 1947–1951
706 Rayner NA, Parker DE, Horton EB, Folland CK, Alexander LV, Rowell DP, Kent EC,
707 Kaplan A (2003) Global analyses of sea surface temperature, sea ice, and night
708 marine air temperature since the late nineteenth century J Geophys Res 108: No.
709 D14, 4407 10.1029/2002JD002670
710 Schmitz WJ (1996) On the world ocean circulation, vol 1. Woods Hole
711 Oceanographic Institute WHOI-96-03, p 141
712 Smith TM, Reynolds RW (2004) Improved extended reconstruction of SST. J Climate
713 17: 2466-2477
714 Stouffer RJ et al (2006) Investigating the causes of the response of the thermohaline
715 circulation to past and future climate changes. J Climate 19: 1365–1387

716 Stouffer RJ, Seidov D, Haupt BJ (2007) Climate Response to External Sources of
717 Freshwater: North Atlantic versus the Southern Ocean. J Climate 20: 436–448
718 Stocker TF, Wright DG, Broecker WS (1992) The influence of high-latitude surface
719 forcing on the global thermohaline circulation. Paleoceanography 7: 529–541
720 Swingedouw D, Fichefet T, Goosse H, Loutre MF (2009) Impact of transient
721 freshwater releases in the Southern Ocean on the AMOC and climate. Clim Dyn
722 33: 365-381
723 Timmermann AM, An S, Krebs U, Goosse H (2005) ENSO suppression due to a
724 weakening of the North Atlantic thermohaline circulation. J Climate 18: 3122–
725 3139
726 Timmermann AM et al (2007) The influence of a weakening of the Atlantic
727 meridional overturning circulation on ENSO. J Climate 20: 4899–4919
728 Ting M, Kushnir Y, Seager R, Li C (2009) Forced and Internal Twentieth-Century
729 SST Trends in the North Atlantic. J Climate 22: 1469–1481
730 Turner J, Comiso JC, Marshall GJ, Lachlan-Cope TA, Bracegirdle T, Maksym T,
731 Meredith MP, Wang Z, Orr A (2009) Non-annular atmospheric circulation
732 change induced by stratospheric ozone depletion and its role in the recent
733 increase of Antarctic sea ice extent, Geophys Res Lett 36: L08502,
734 doi:10.1029/2009GL037524
735 Vecchi GA, Clement A, Soden BJ (2008) Examining the Tropical Pacific's Response
736 to Global Warming. Eos Trans 89: 81–83

737 Vellinga M, Wood R, Gregory JM (2002) Processes governing the recovery of a
738 perturbed thermohaline circulation in HadCM3. J Climate 15: 764–779
739 Weaver AJ, Saenko OA, Clark PU, Mitrovica JX (2003) Meltwater pulse 1A from
740 Antarctic as a trigger of the Bølling-Allerød warm interval. Science 299: 1709–
741 1713
742 Wang C, Zhang L (2013) Multidecadal Ocean Temperature and Salinity Variability in
743 the Tropical North Atlantic: Linking with the AMO, AMOC, and Subtropical
744 Cell. J Climate 26: 6137–6162
745 Wang XF, Auler AS, Edwards RL, Cheng H, Cristalll PS, Smart PL, Richards DA,
746 Shen CC (2004) Wet periods in northeastern Brazil over the past 210 kyr linked
747 to distant climate anomalies. Nature 432: 740–743
748 Wang YJ, Cheng H, Edwards RL, An ZS, Wu JY, Shen CC, Dorale JA (2001) A
749 high-resolution absolute-dated late Pleistocene monsoon record from Hulu Cave,
750 China. Science 294: 2345–2348
751 Wang Z, Zhang X, Guan Z, Sun B, Yang X, Liu C (2015) An atmospheric origin of
752 the multi-decadal bipolar seesaw. Sci. Rep. 5, 8909
753 Wunsch C, Heimbach P (2006) Estimated Decadal Changes in the North Atlantic
754 Meridional Overturning Circulation and Heat Flux 1993–2004. J Phys Oceanogr
755 36: 2012–2024
756 Wu L, Li C, Yang C, Xie SP (2008) Glo bal Teleconnections in Response to a
757 Shutdown of the Atlantic Meridional Overturning Circulation. J Climate 21:
758 3002–3019

759 Zhang L, Wu L, Yu L (2011) Oceanic origin of a recent La Niña-like trend in the
760 tropical Pacific. Adv Atmos Sci 28: 1109–1117
761 Zhang L, Wang C (2013) Multidecadal North Atlantic sea surface temperature and
762 Atlantic meridional overturning circulation variability in CMIP5 historical
763 simulations. J Geophys Res Oceans 118: 5772–5791
764 Zhang R (2010) Latitudinal dependence of Atlantic Meridional Overturning
765 Circulation (AMOC) variations. Geophysical Research Letters 37: L16703,
766 doi:10.1029/2010GL044474
767 Zhang R, Delworth TL (2005) Simulated tropical response to a substantial weakening
768 of the Atlantic thermohaline circulation. Journal of Climate 18: 1853–1860.
769 Zhang S, Harrison MJ, Rosati A, Wittenberg A (2007) System Design and Evaluation
770 of Coupled Ensemble Data Assimilation for Global Oceanic Climate Studies.
771 Mon Wea Rev 135: 3541–3564.
772
773

Figure Captions:

Figure 1: Spatial pattern of the heat flux anomalies (W m^{-2}, positive downward) used as anomalous flux forcing in the model experiments. The flux is calculated from the ECMWF-Interim reanalysis, and is the mean flux over Dec-March that corresponds to one standard deviation of the North Atlantic Oscillation in observation.

Figure 2: Latitude-depth section of the meridional overturning streamfunction in the Atlantic Ocean (north of 32ºS) and in the Southern Ocean (south of 32ºS). The contour internal is 4 Sv. Red shading denotes positive values representing clockwise circulation; blue denotes negative values representing anticlockwise circulation. Shown are the long term mean streamfunction in the (a) fully coupled GFDL CM2.1 control run (Delworth et al. 2006) and (b) ECDA reanalysis (Zhang et al. 2007). The white line superimposed in (a) denotes the zonally averaged 27.6 kg/m^3 isopycnal. (c) Long term mean surface wind stress (N/m^2) in the fully coupled control simulation.

Figure 3: (a) Annual mean extratropical AMOC (red line), AABW (blue line) and Deacon Cell (green line) responses to the 100-yr periodic NAO flux forcing. The AMOC index is defined as the maximum Atlantic streamfunction in the 20ºN-60ºN band and below 500-m. The AABW cell is denoted as the absolute value of the minimum global streamfunction south of 60ºS. The maximum global streamfunction between 60ºS and 40ºS represents the strength of the Deacon cell. Both the unfiltered and 30-yr low pass filtered indexes are shown. Unit is Sv. (b) Same as (a) but for the percentage change (response divided by the long term mean value). (c) Regression of the mixed layer depth (MLD) against the normalized 30-yr low pass filtered AMOC index. Unit is m.

Figure 4: Shown are the zonally averaged (60ºW-20ºE) 27.6 kg/m^3 isopycnal depth response (30-yr low pass filtered) to the 100-yr periodic NAO flux forcing. Unit is m.

Figure 5: Time series of annual mean responses to the 100-year periodic NAO flux forcing. (a) Red line denotes the AMOC in the extratropical North Atlantic (20º-60ºN), green line denotes the AMOC in the tropical North Atlantic (0º-20ºN) , and the blue line denotes the SST averagd over 0º-70ºN, and from coast to coast. (b) AABW (magenta line), Deacon Cell (yellow line) and area averaged Southern Ocean (80º-20ºS, coast to coast) SST (baby blue line). Units are Sv for the MOC and 0.1 ºC for the SST. All data are 30-yr low pass filtered to retain low frequency variability.

Figure 6: Spatial patterns of simulated temperature bipolar seesaw response to the 100-yr periodic NAO forcing. (a) Regression of annually-averaged zonal mean (0º-360ºE) temperature response upon the 30-yr low pass filtered Southern Ocean (90º-40ºS) area averaged SST index. Unit is ºC/ºC. (b) Regression of annually-averaged SST (shading) and SLP (contours, contour interval is 0.3) responses upon the 30-yr low pass filtered North Atlantic (0ºN-70ºN, coast to coast) area averaged SST index. Units are ºC/ºC for SST and hPa/ºC for SLP. (c) SLP response (contour interval: 0.3hPa) to the Southern Ocean SST cooling anomaly south of 50ºS in (b) which we imposed in the fully coupled model.

Figure 7: Shown are the regressions of (a) annual and (b) austral winter mean sea ice concentration (shading)/SLP (contours) responses versus the 30-yr low pass filtered Southern Ocean (90ºS-40ºS) area averaged SST index in response to the 100-yr periodic NAO forcing. The results are multiplied by -1. Units are 100%/ºC for the sea ice concentration and hPa/ºC for the SLP. The contour interval is 0.3 hPa/ºC for SLP.

Figure 8: (a) Regression coefficients of wind stress (vector) and wind stress curl (shading) responses versus the 30-yr low pass filtered North Atlantic (0º-70ºN) area averaged SST index in the 100-yr periodic NAO forcing experiment. (b) Same as (a) but for the wind stress and surface net heat flux (positive downward). Units for the wind stress, wind stress curl and net heat flux are $N/m^2/ºC$, $10^{-7}N/m^3/ºC$ and $W/m^2/ºC$, respectively. (c) Unfiltered and 30-yr low pass filtered time series of Weddell Sea area averaged (77ºS-65ºS, 60ºW-10ºE) net heat flux (W/m^2), turbulent heat flux (W/m^2) and the AABW cell (Sv) responses.

Figure 9: Time evolution of various quantities responses to a sudden switch on of heat flux anomaly corresponding to a one standard deviation increase of NAO. (a) AMOC and AABW cell (Sv) responses. (b) Weddell Sea (77ºS-65ºS, 60ºW-10ºE) area averaged net heat flux (W/m^2) and the AABW cell (Sv) responses. (c) Weddell Sea area averaged net heat flux, turbulent and radiative heat flux (W/m^2) responses.

Figure 10: Time averaged response to a sudden switch on of heat flux anomaly corresponding to a one standard deviation increase of the NAO. (a) Global meridional overturning circulation (GMOC, contour interval is 0.15 Sv) and Atlantic zonal mean temperature (ºC, shading) responses averaged from year 51 to150. (b) SST (ºC, shading) and surface net heat flux (W/m^2, contours) responses averaged from year 31 to 50. (c) Wind stress (N/m^2, vector) and wind stress curl (N/m^3 shading) responses averaged from year 31 to 50.

Figure 11: Time evolution of Atlantic (80ºW-20ºE) zonal mean density (kg/m^3) response to a sudden switch on of heat flux anomaly corresponding to a one standard deviation increase of the NAO.

Figure 12: (a) Annually SST (ºC, shading) and SLP (hPa, contour interval: 0.06 hPa) responses in "Restore_NASST" run in which we impose a North Atlanitc (0º-70ºN, coast to coast) SST warming anomaly in the coupled model. (b) Zonal mean (0ºE-0ºW) troposphere temperature (K, shading) response to the anomalous North Atlantic SST warming. The black contours overlapped in (b) denote the long term mean zonal mean temperature (K).

Figure 13: Time series of annually Southern Ocean (0º-360ºE, 70º-50ºS) and extratropical North Atlantic (300º-350ºE, 50º-65ºN) area averaged SST (ºC) anomaly from 1961 to 2013 in (a) HadISST (Rayner et al. 2003), (b) ERSST (Smith and Reynolds 2004), (c) Ishii (Ishii et al. 2005), and (d) ECDA (Zhang et al. 2007). The anomaly is derived by subtracting the mean value in period 1961-2013. The red and blue lines denote the original and internal SST variations in the Southern Ocean, with their magnitudes denoted in the left side of y-axis. The magenta and green lines denote the original and internal SST variations in the extratropical North Atlantic, with their

861 magnitudes denoted in the right side of y-axis.
862
863 **Figure 14**: Annually SST(ºC) and SLP(hPa) differences between period 1996-2013 and
864 1979-1995 in (a) HadISST/20CRv2, (b) ERSST, (c) Ishii and (d) ECDA datasets. Contour interval
865 is 0.4hPa for SLP.
866
867 **Figure 15**: Annually Southern Ocean column averaged (0º-360ºE, 90º-60ºS, 200-1500m)
868 subsurface temperature anomaly in (a) Ishii and (b) ECDA data from 1961 to 2013. The anomaly
869 is derived by subtracting the mean value in period 1961-2013. Latitude-depth section of the zonal
870 mean (0º-360ºE) temperature difference between 1996-2013 and 1979-1995 in (c) Ishii and (d)
871 ECDA reanalysis. Unit is ºC.
872
873 **Figure 16**: (a) Time series of annually AMOC, AABW and Deacon cell anomalies from 1961 to
874 2013 in ECDA reanalysis. Unit is Sv. (b) Same as (a) but for the ensemble mean results in the
875 GFDL CM2.1 historical run. (c) Difference between (a) and (b).
876
877 **Figure 17**: Austral winter (a), summer (b) and annual mean (c) sea ice concentration (HadISST)
878 and SLP (20CRv2, contour interval: 0.4) differences between period 1996-2013 and 1979-1995.
879 Units are 100% for the sea ice and hPa for the SLP. The yellow contour indicates the absolute
880 value of sea ice concentration inside is larger than 0.1.
881

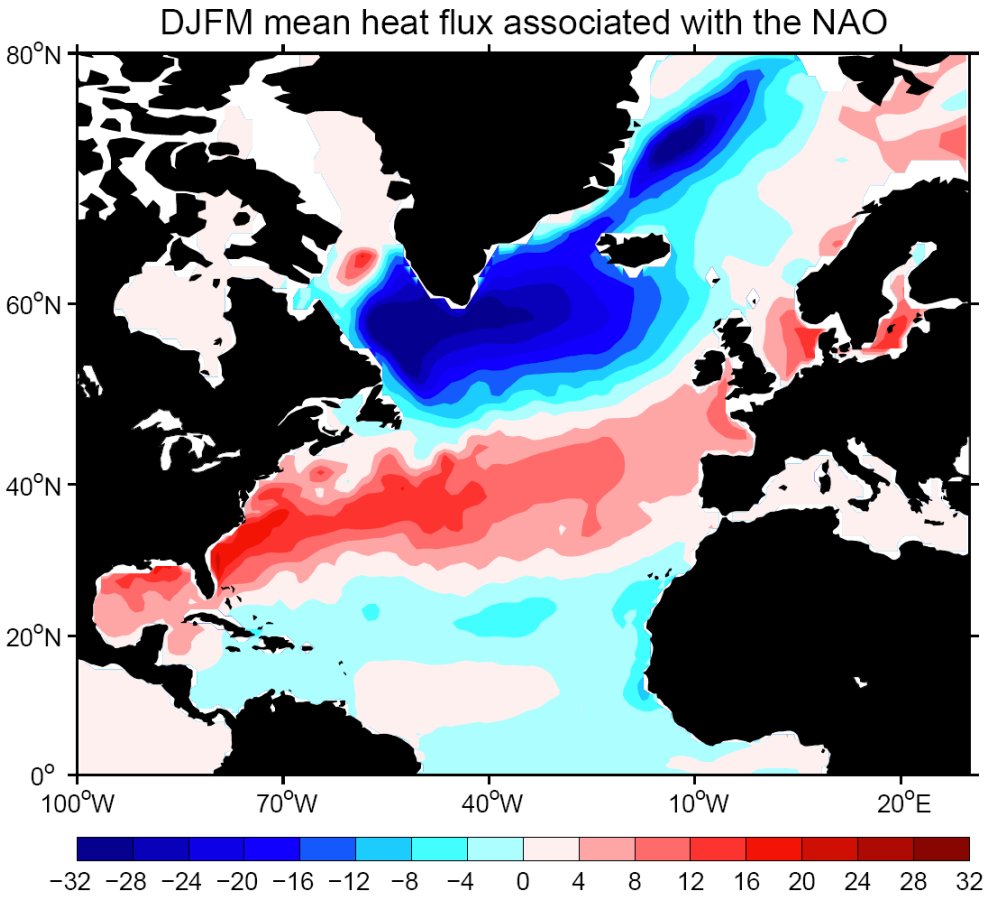

882
883
884 **Figure 1**: Spatial pattern of the heat flux anomalies (W m^{-2}, positive downward) used as
885 anomalous flux forcing in the model experiments. The flux is calculated from the
886 ECMWF-Interim reanalysis, and is the mean flux over Dec-March that corresponds to one
887 standard deviation of the North Atlantic Oscillation in observation.
888

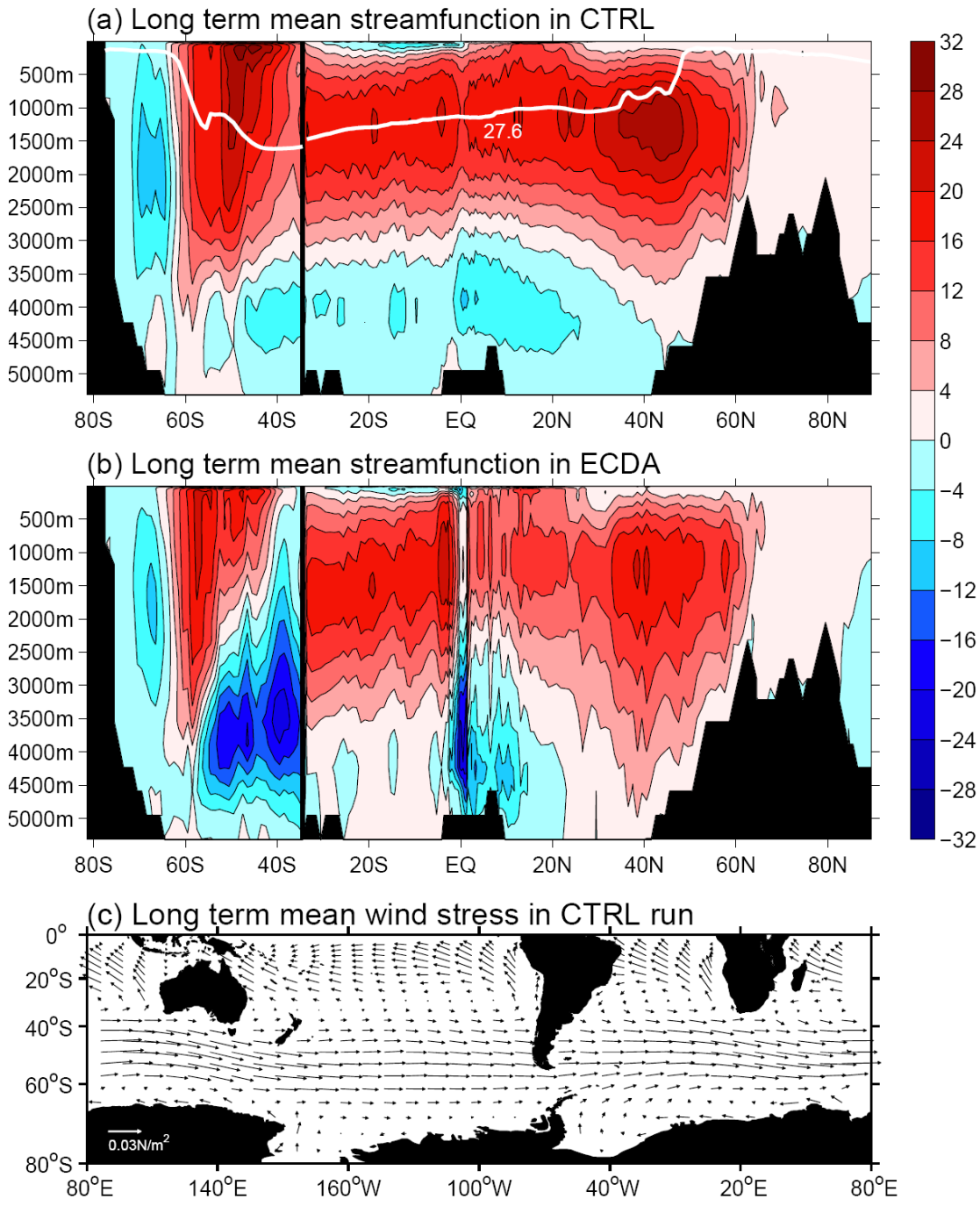

Figure 2: Latitude-depth section of the meridional overturning streamfunction in the Atlantic Ocean (north of 32°S) and in the Southern Ocean (south of 32°S). The contour internal is 4 Sv. Red shading denotes positive values representing clockwise circulation; blue denotes negative values representing anticlockwise circulation. Shown are the long term mean streamfunction in the (a) fully coupled GFDL CM2.1 control run (Delworth et al. 2006) and (b) ECDA reanalysis (Zhang et al. 2007). The white line superimposed in (a) denotes the zonally averaged 27.6 kg/m^3 isopycnal. (c) Long term mean surface wind stress (N/m^2) in the fully coupled control simulation.

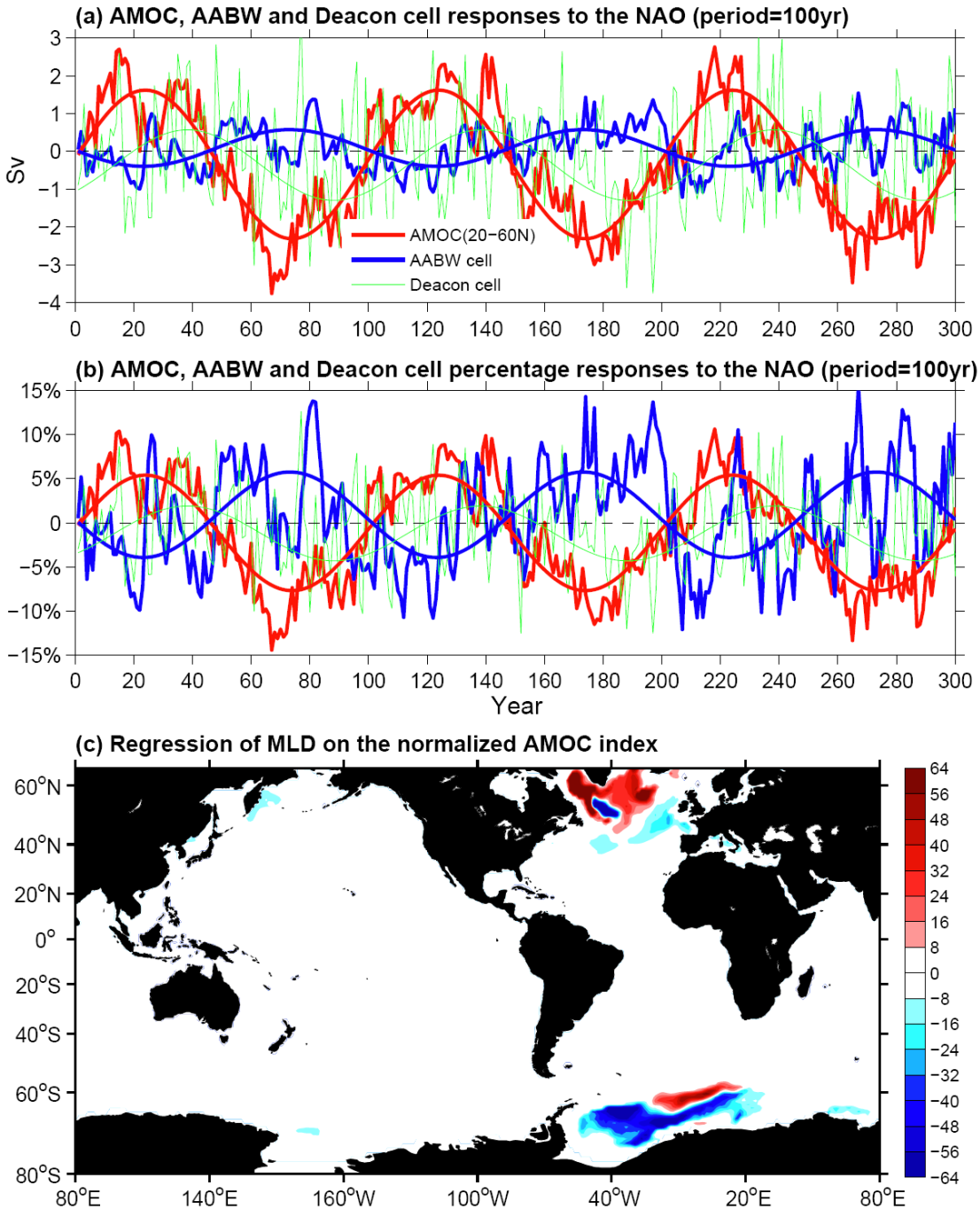

Figure 3: (a) Annual mean extratropical AMOC (red line), AABW (blue line) and Deacon Cell (green line) responses to the 100-yr periodic NAO flux forcing. The AMOC index is defined as the maximum Atlantic streamfunction in the 20°N-60°N band and below 500-m. The AABW cell is denoted as the absolute value of the minimum global streamfunction south of 60°S. The maximum global streamfunction between 60°S and 40°S represents the strength of the Deacon cell. Both the unfiltered and 30-yr low pass filtered indexes are shown. Unit is Sv. (b) Same as (a) but for the percentage change (response divided by the long term mean value). (c) Regression of the mixed layer depth (MLD) against the normalized 30-yr low pass filtered AMOC index. Unit is m.

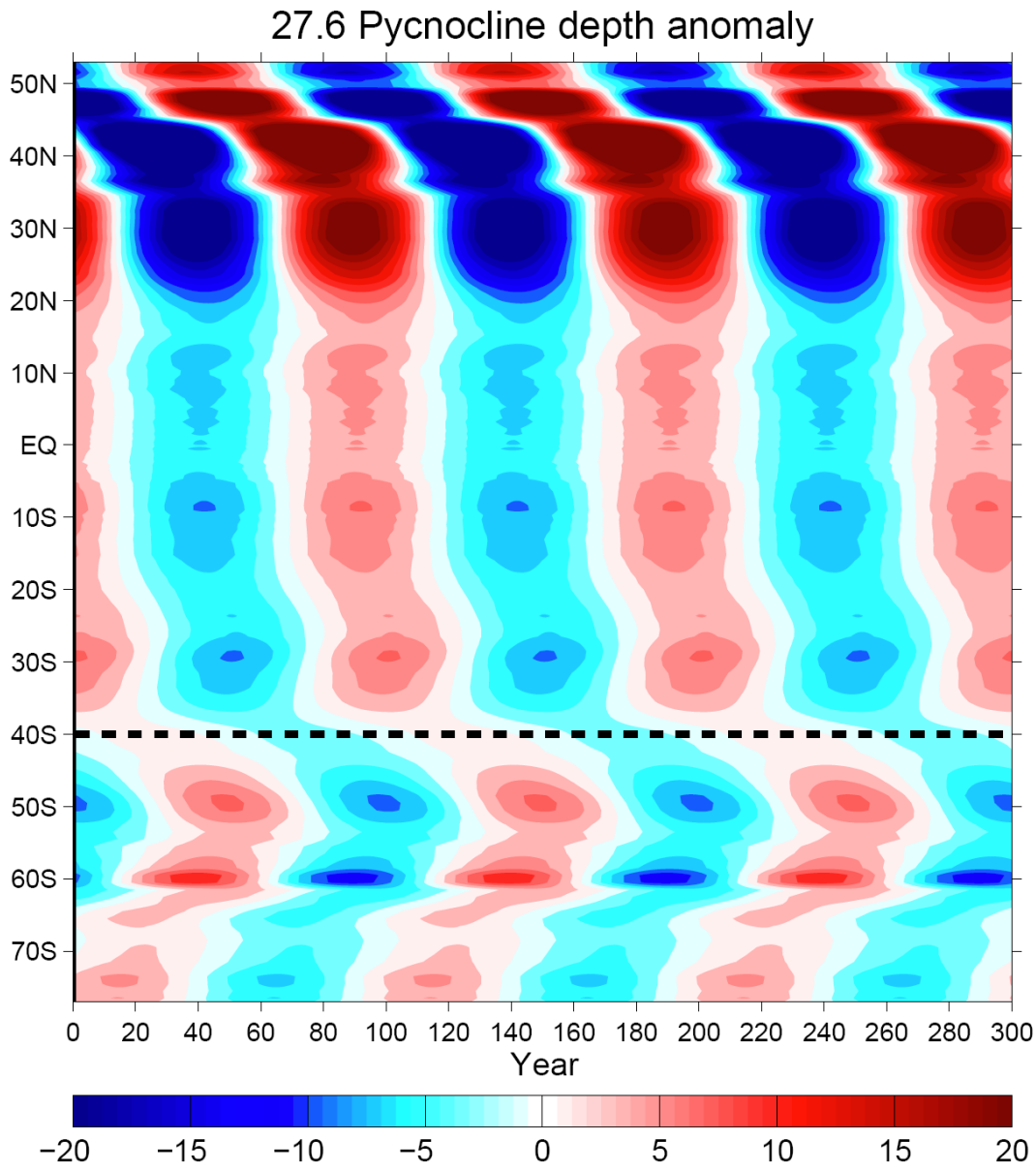

Figure 4: Shown are the zonally averaged (60°W-20°E) 27.6 kg/m^3 isopycnal depth response (30-yr low pass filtered) to the 100-yr periodic NAO flux forcing. Unit is m.

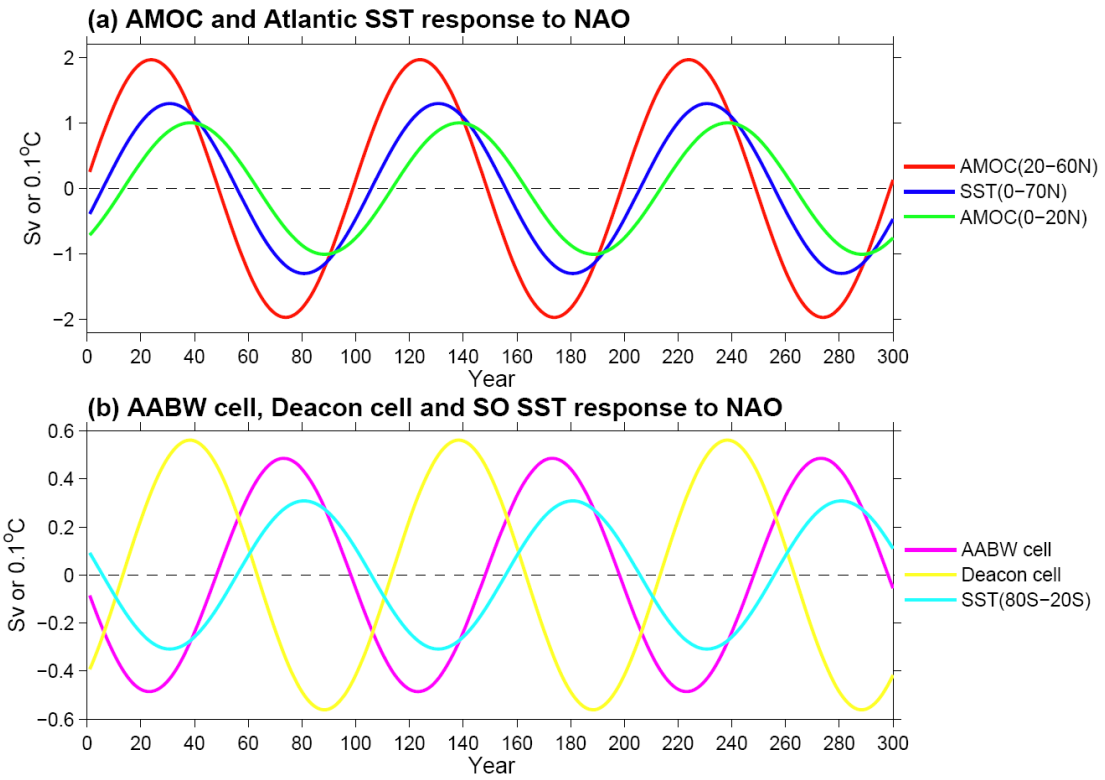

Figure 5: (a) Annually extratropical (20º-60ºN) AMOC (red line), tropical (0º-20ºN) AMOC (green line) and North Atlantic (0º-70ºN, coast to coast) area averaged SST (blue line) responses to the 100-yr periodic NAO flux forcing. (b) Annually AABW (magenta line), Deacon Cell (yellow line) and area averaged Southern Ocean (80º-20ºS, coast to coast) SST (baby blue line) responses. Units are Sv for the MOC and 0.1 ºC for the SST. All data are 30-yr low pass filtered to retain low frequency variability.

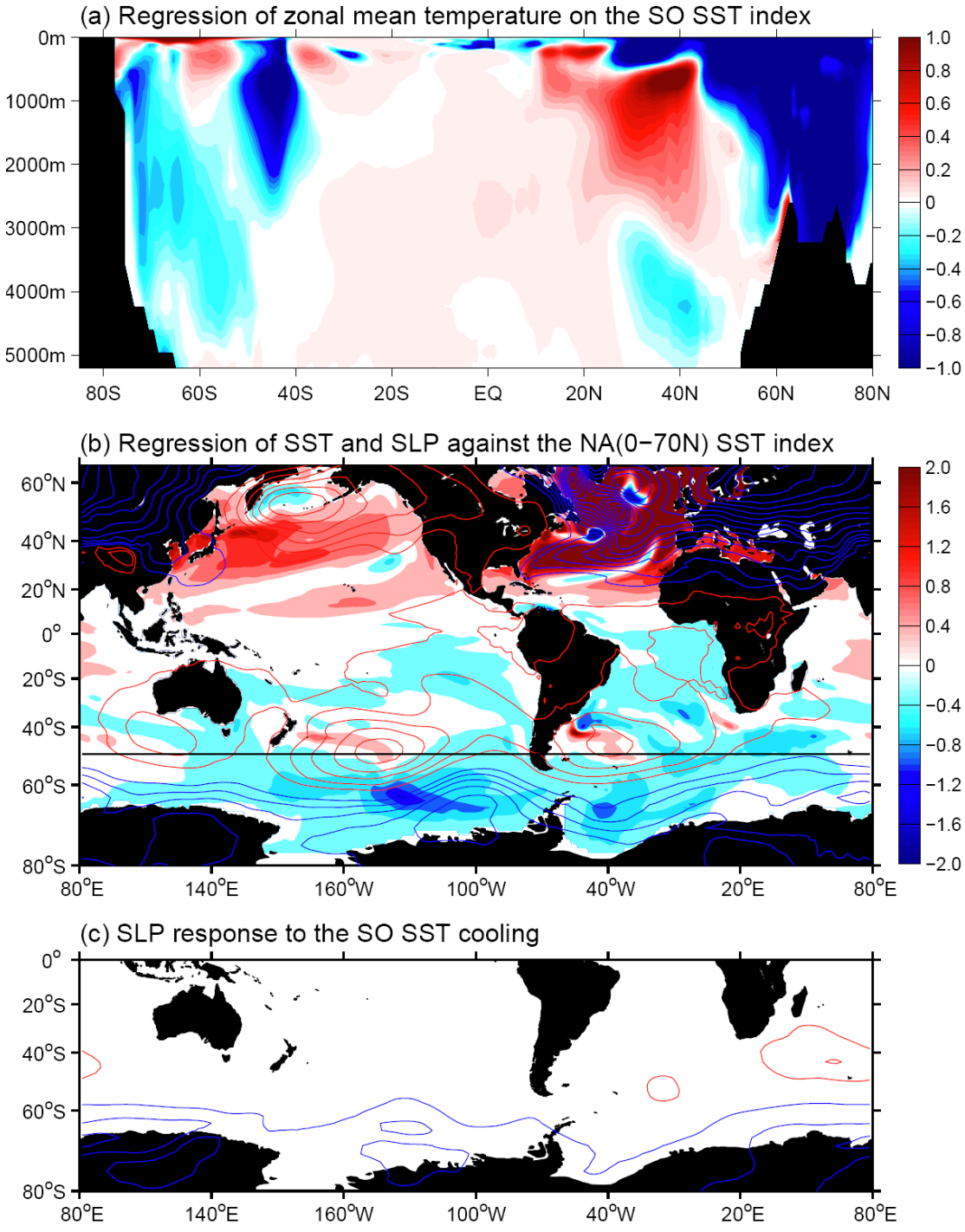

Figure 6: Spatial patterns of simulated temperature bipolar seesaw response to the 100-yr periodic NAO forcing. (a) Regression of annually zonal mean (0º-360ºE) temperature response upon the 30-yr low pass filtered Southern Ocean (90º-40ºS) area averaged SST index. Unit is ºC/ºC. (b) Regression of annually SST (shading) and SLP (contours, contour interval is 0.3) responses upon the 30-yr low pass filtered North Atlantic (0ºN-70ºN, coast to coast) area averaged SST index. Units are ºC/ºC for SST and hPa/ºC for SLP. (c) SLP response (contour interval: 0.3hPa) to the Southern Ocean SST cooling anomaly south of 50ºS in (b) which we imposed in the fully coupled model.

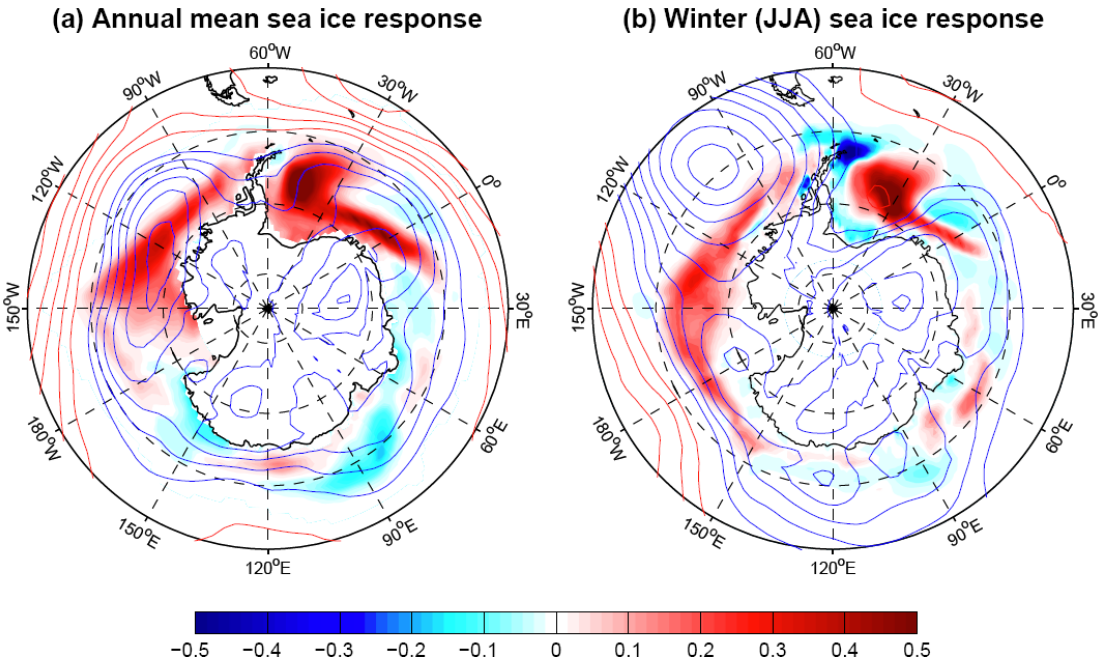

Figure 7: Shown are the regressions of (a) annual and (b) austral winter mean sea ice concentration (shading)/SLP (contours) responses versus the 30-yr low pass filtered Southern Ocean (90°S-40°S) area averaged SST index in response to the 100-yr periodic NAO forcing. The results are multiplied by -1. Units are 100%/°C for the sea ice concentration and hPa/°C for the SLP. The contour interval is 0.3 hPa/°C for SLP.

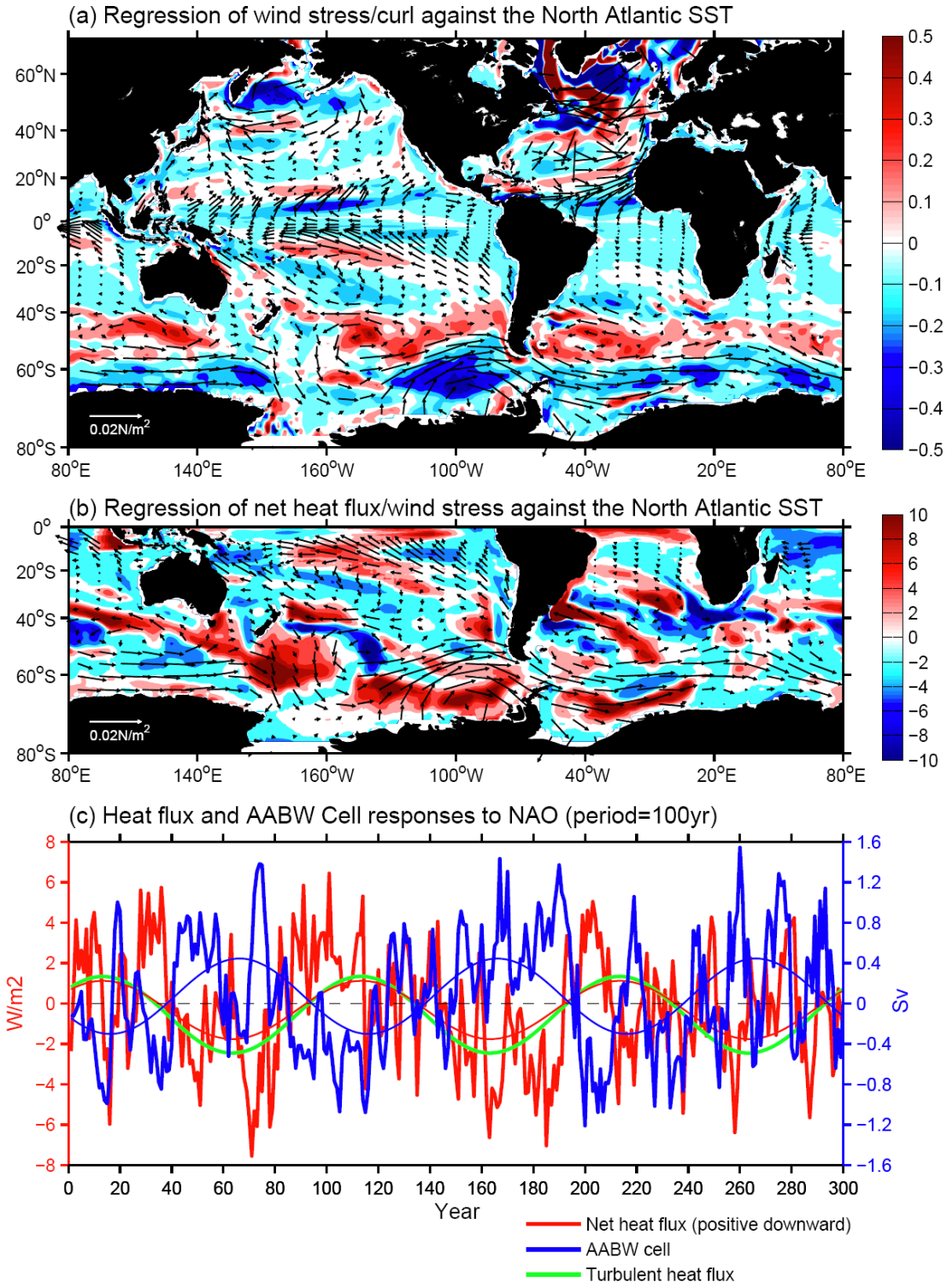

Figure 8: (a) Regression coefficients of wind stress (vector) and wind stress curl (shading) responses versus the 30-yr low pass filtered North Atlantic (0°-70°N) area averaged SST index in the 100-yr periodic NAO forcing experiment. (b) Same as (a) but for the wind stress and surface net heat flux (positive downward). Units for the wind stress, wind stress curl and net heat flux are $N/m^2/°C$, $10^{-7}N/m^3/°C$ and $W/m^2/°C$, respectively. (c) Unfiltered and 30-yr low pass filtered time series of Weddell Sea area averaged (77°S-65°S, 60°W-10°E) net heat flux (W/m^2), turbulent heat flux (W/m^2) and the AABW cell (Sv) responses.

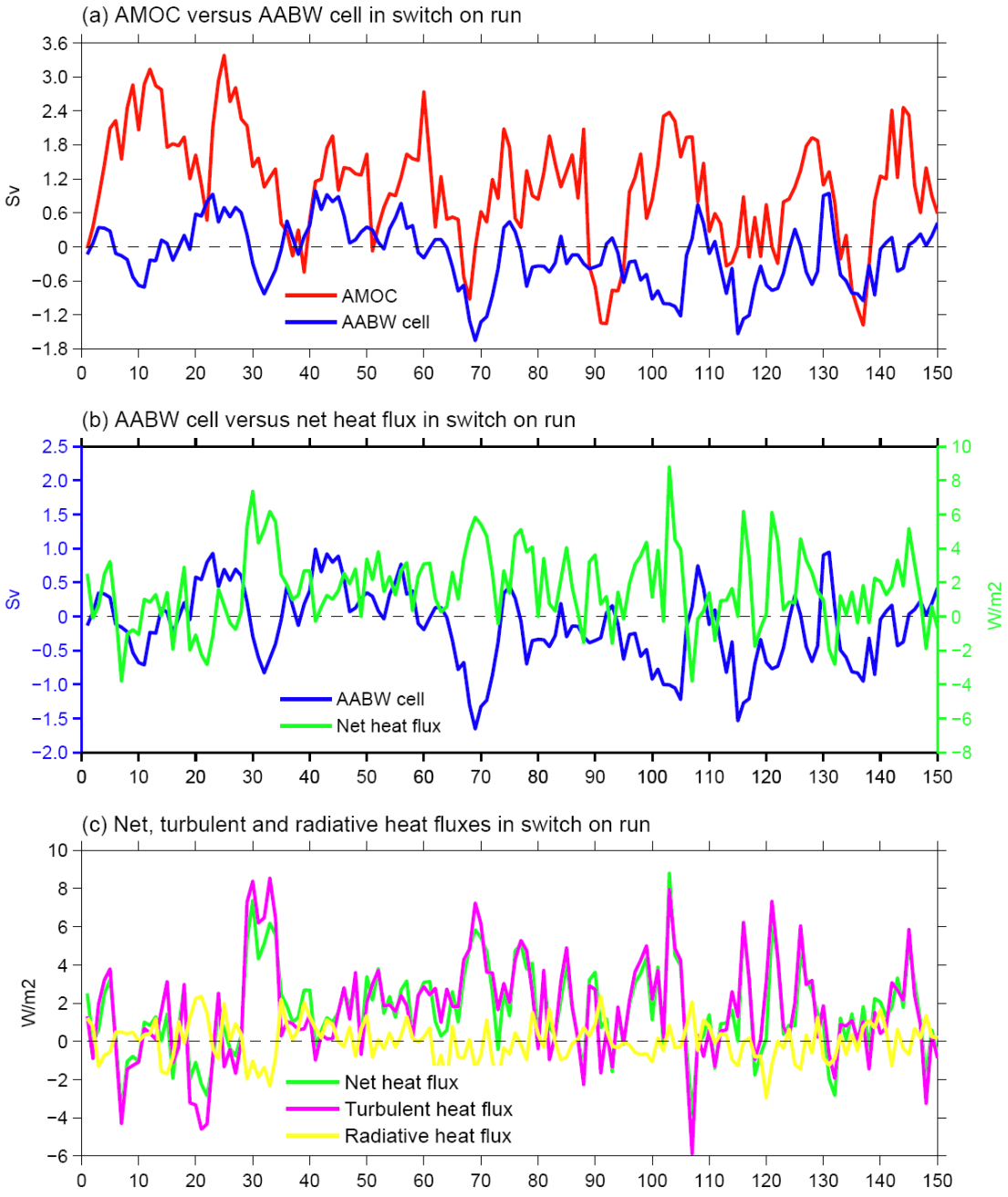

Figure 9: Time evolution of various quantities responses to a sudden switch on of heat flux anomaly corresponding to a one standard deviation increase of NAO. (a) AMOC and AABW cell (Sv) responses. (b) Weddell Sea (77°S-65°S, 60°W-10°E) area averaged net heat flux (W/m^2) and the AABW cell (Sv) responses. (c) Weddell Sea area averaged net heat flux, turbulent and radiative heat flux (W/m^2) responses.

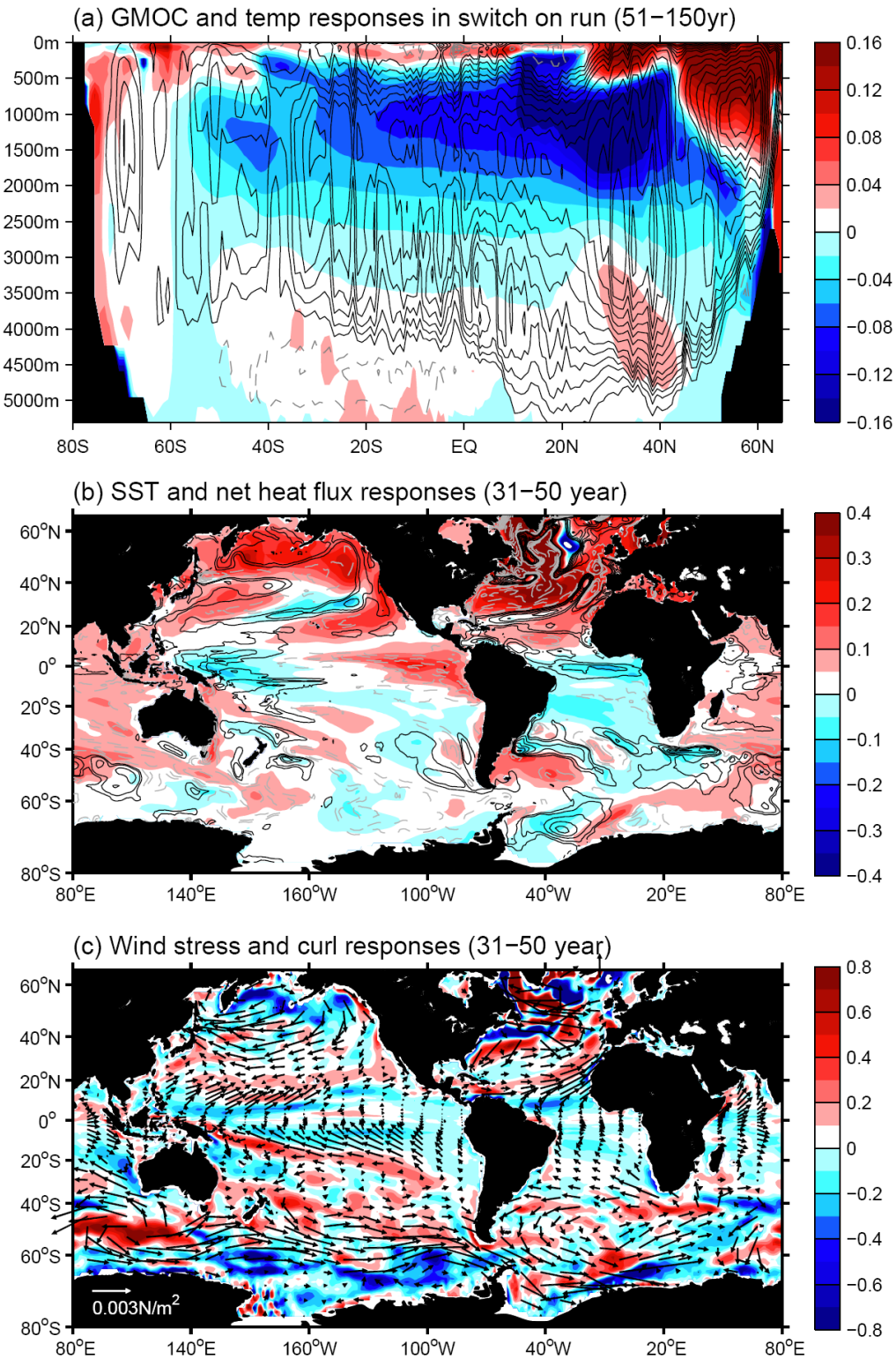

Figure 10: Time averaged response to a sudden switch on of heat flux anomaly corresponding to a one standard deviation increase of the NAO. (a) Global meridional overturning circulation (GMOC, contour interval is 0.15 Sv) and Atlantic zonal mean temperature (°C, shading) responses averaged from year 51 to150. (b) SST (°C, shading) and surface net heat flux (W/m^2, contours) responses averaged from year 31 to 50. (c) Wind stress (N/m^2, vector) and wind stress curl (N/m^3 shading) responses averaged from year 31 to 50.

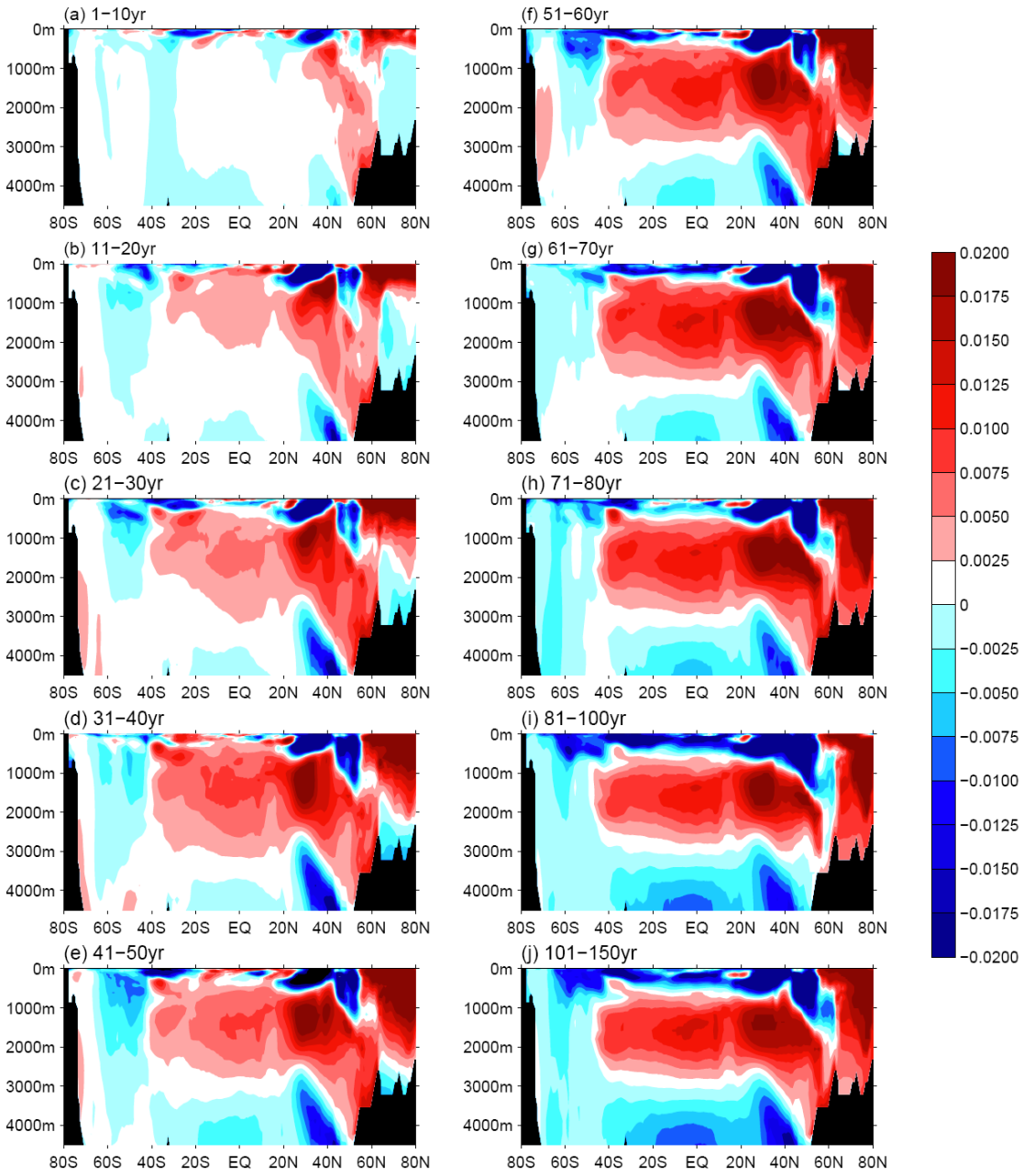

Figure 11: Time evolution of Atlantic (80°W-20°E) zonal mean density (kg/m^3) response to a sudden switch on of heat flux anomaly corresponding to a one standard deviation increase of the NAO.

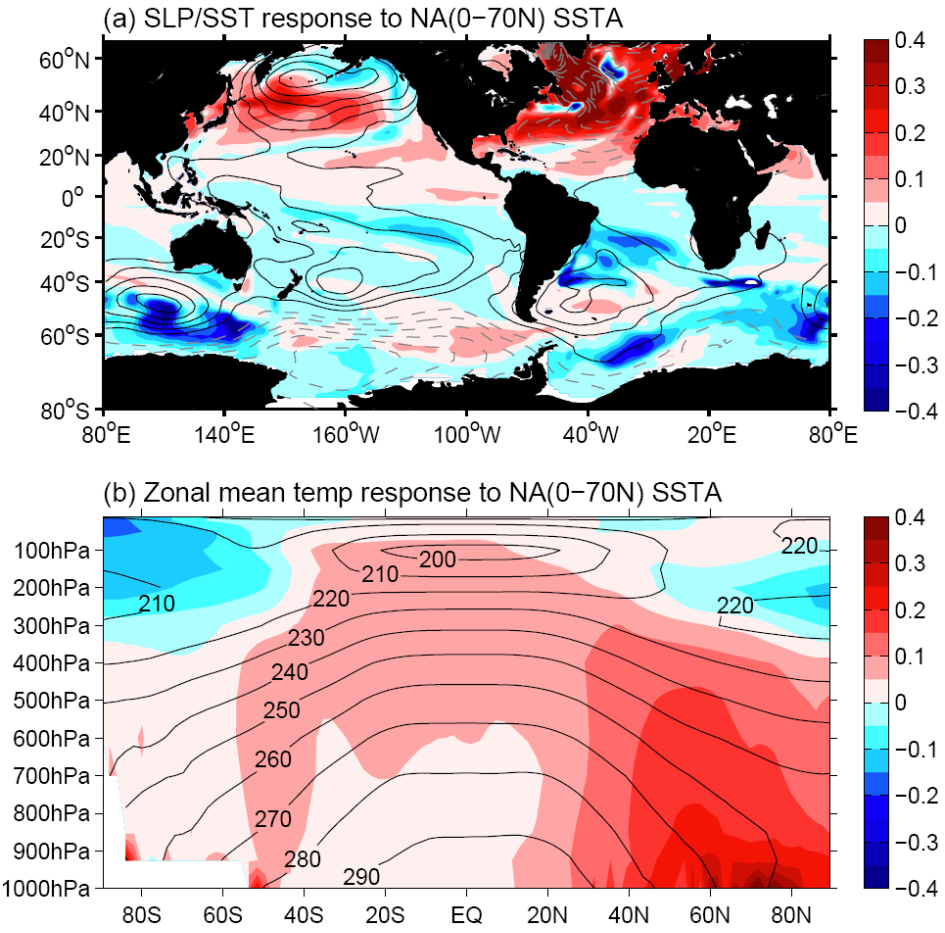

975

976

977 **Figure 12**: (a) Annually SST (°C, shading) and SLP (hPa, contour interval: 0.06 hPa) responses in
978 "Restore_NASST" run in which we impose a North Atlanitc (0°-70°N, coast to coast) SST
979 warming anomaly in the coupled model. (b) Zonal mean (0°E-0°W) troposphere temperature (K,
980 shading) response to the anomalous North Atlantic SST warming. The black contours overlapped
981 in (b) denote the long term mean zonal mean temperature (K).

982

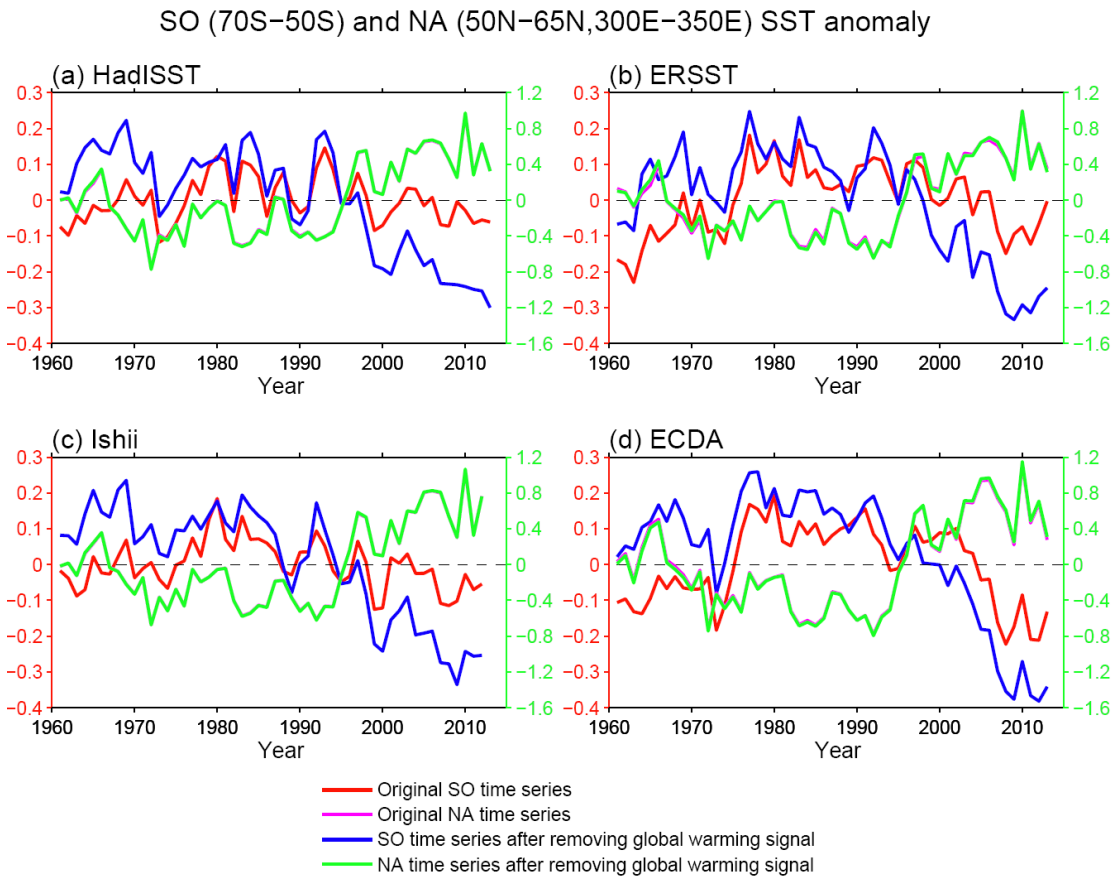

983

984

985 **Figure 13**: Time series of annually Southern Ocean (0º-360ºE, 70º-50ºS) and extratropical North
986 Atlantic (300º-350ºE, 50º-65ºN) area averaged SST (ºC) anomaly from 1961 to 2013 in (a)
987 HadISST (Rayner et al. 2003), (b) ERSST (Smith and Reynolds 2004), (c) Ishii (Ishii et al. 2005),
988 and (d) ECDA (Zhang et al. 2007). The anomaly is derived by subtracting the mean value in
989 period 1961-2013. The red and blue lines denote the original and internal SST variations in the
990 Southern Ocean, with their magnitudes denoted in the left side of y-axis. The magenta and green
991 lines denote the original and internal SST variations in the extratropical North Atlantic, with their
992 magnitudes denoted in the right side of y-axis.

993

994

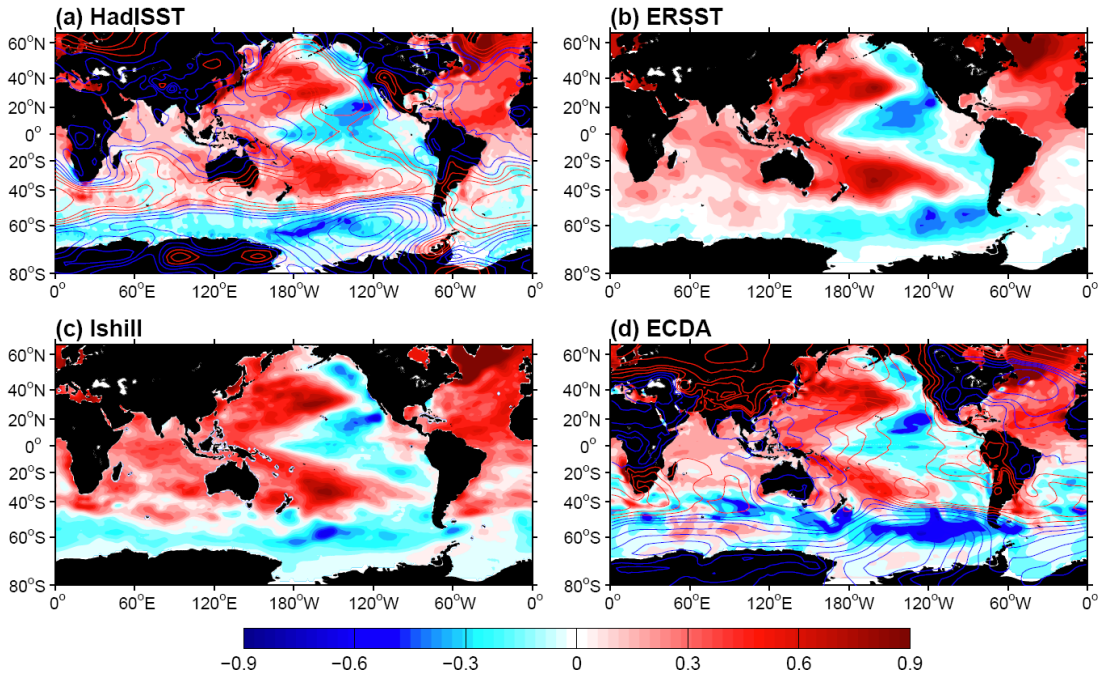

Figure 14: Annually SST(°C) and SLP(hPa) differences between period 1996-2013 and 1979-1995 in (a) HadISST/20CRv2, (b) ERSST, (c) Ishii and (d) ECDA datasets. Contour interval is 0.4hPa for SLP.

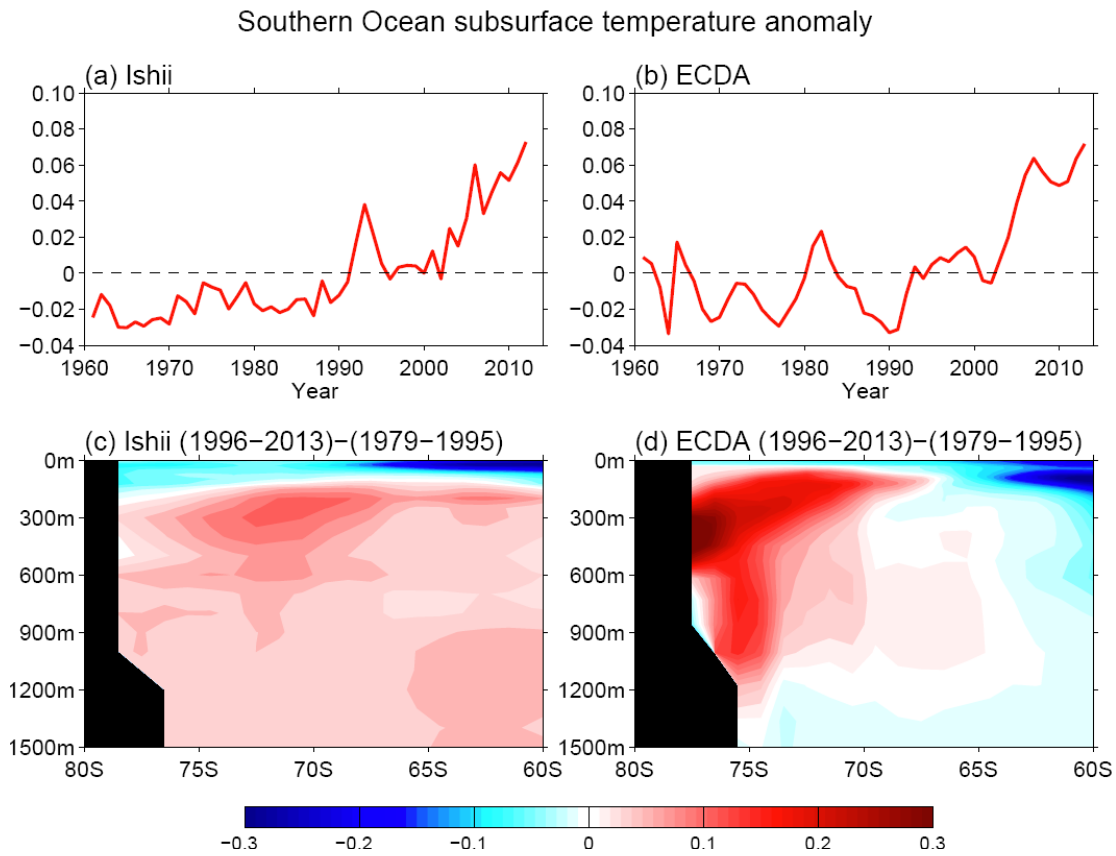

Figure 15: Annually Southern Ocean column averaged (0º-360ºE, 90º-60ºS, 200-1500m) subsurface temperature anomaly in (a) Ishii and (b) ECDA data from 1961 to 2013. The anomaly is derived by subtracting the mean value in period 1961-2013. Latitude-depth section of the zonal mean (0º-360ºE) temperature difference between 1996-2013 and 1979-1995 in (c) Ishii and (d) ECDA reanalysis. Unit is ºC.

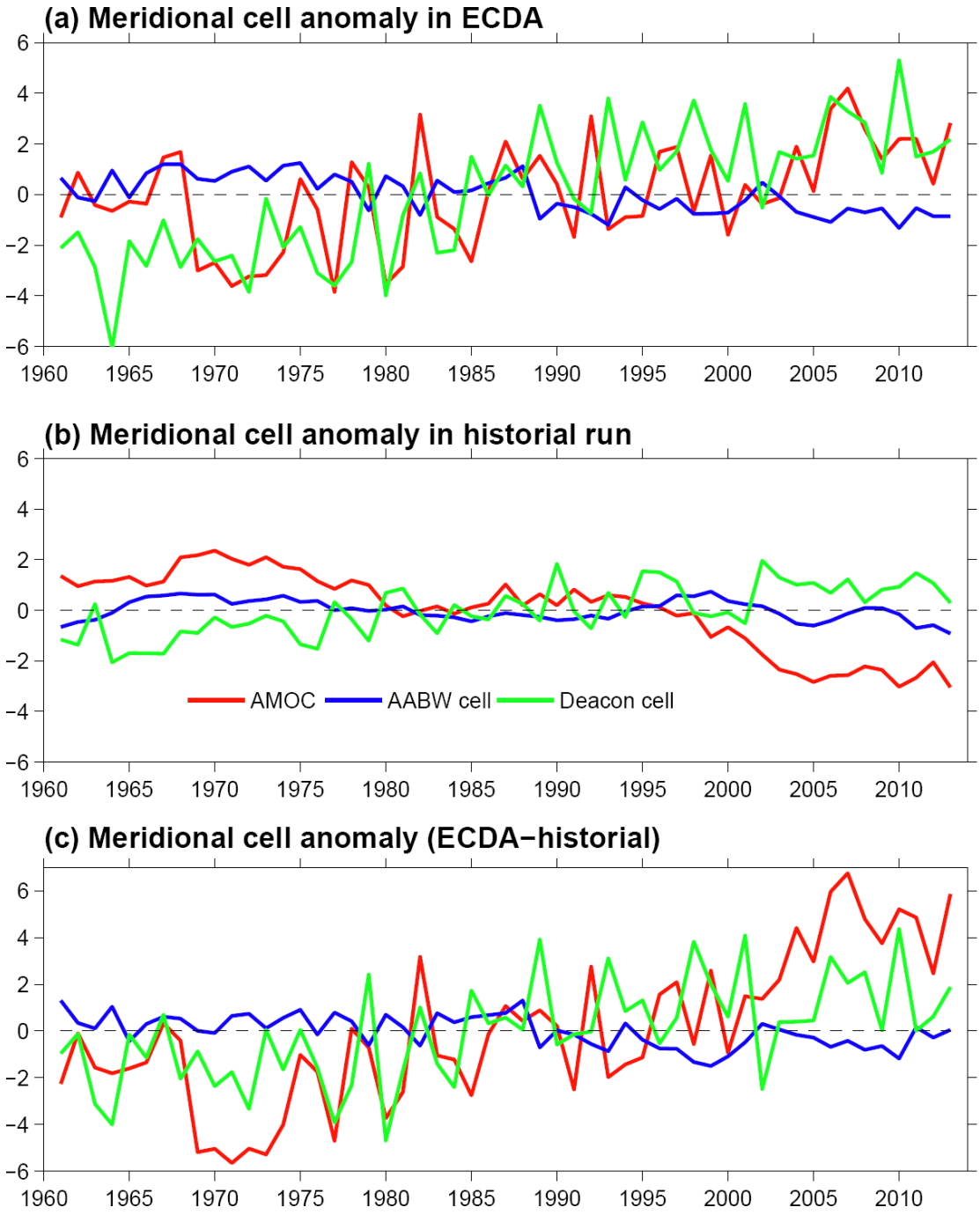

Figure 16: (a) Time series of annually AMOC, AABW and Deacon cell anomalies from 1961 to 2013 in ECDA reanalysis. Unit is Sv. (b) Same as (a) but for the ensemble mean results in the GFDL CM2.1 historical run. (c) Difference between (a) and (b).

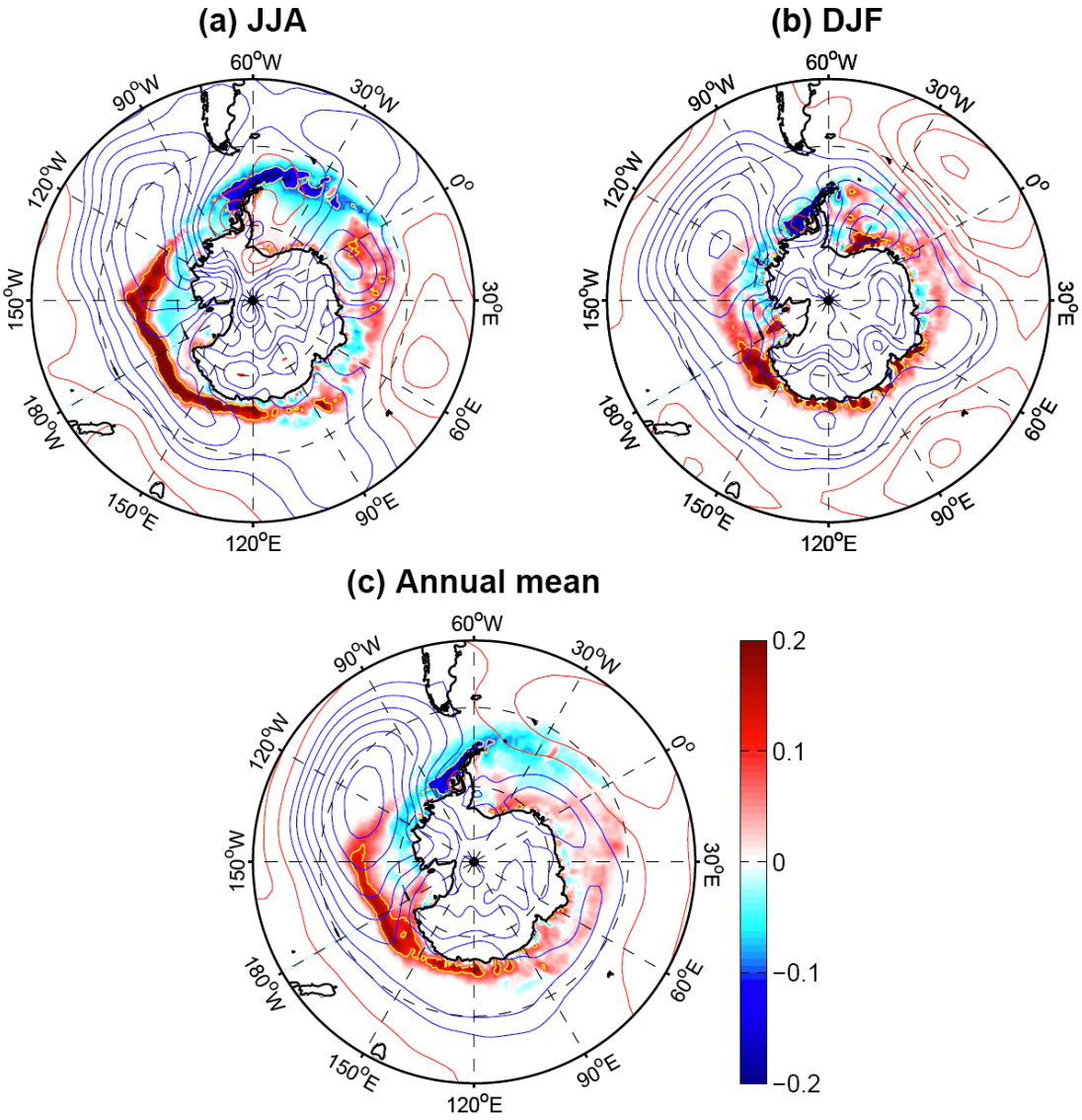

Figure 17: Austral winter (a), summer (b) and annual mean (c) sea ice concentration (HadISST) and SLP (20CRv2, contour interval: 0.4) differences between period 1996-2013 and 1979-1995. Units are 100% for the sea ice and hPa for the SLP. The yellow contour indicates the absolute value of sea ice concentration inside is larger than 0.1.